Utrecht University

Royal Netherlands Institute for Sea Research

MASTER THESIS

Ferry-ADCP observations of tidal currents in the Marsdiep inlet and how they are affected by the motion of the ferry

Author:
Athina Karaoli

Supervisors:
Prof. Dr. Leo R.M. Maas
Dr. Ir. Johan van der Molen
Dr. Sjoerd Groeskamp

A thesis submitted in fulfillment of the requirements for the degree of Master of Climate Physics which is carried out at Institute for Marine and Atmospheric Research Utrecht (IMAU) in cooperation with Royal Netherlands Institute for Sea Research (NIOZ)

October 14, 2022

Abstract

The Wadden Sea is a dynamic tidal system with multiple inlets. In the western Dutch Wadden Sea large amounts of fresh water coming from Lake IJssel are being exchanged with saline water coming from the North Sea during a tidal cycle. This study analyzes the tidal currents in the Marsdiep inlet which is located between the mainland of the Netherlands and the island of Texel. The velocity measurements are obtained via two Acoustic Doppler Current Profilers (ADCPs) mounted underneath the hull near the bow and the stern of the Texels Eigen Stoomboot Onderneming (TESO) ferry. The use of two ADCPs allows to investigate not only the spatial and the temporal variability of the velocity field of the flow but also the turbulence during tidal cycles. Features of tidally induced turbulence are identified by using the difference of the measurements of the horizontal velocities of the two ADCPs which were found to differ slightly. In this study, the vertical profile of the turbulence as well as its relation with the strength and the phase of the tide are investigated. Regarding the vertical velocity of the flow, it is observed that the ADCP at the bow of the ferry always measures a downwelling motion while the ADCP at the stern of the ferry measures an upwelling motion of the flow. This observation leads to the speculation that the ferry's motion influences the velocity measurements and the measured velocities are not the real ones. A correction of the vertical velocity component for the ferry's motion is introduced in this study and through this correction a physical interpretation of the vertical velocity is given by identifying physical features in the inlet. Finally, we expect that the component of the velocity along the sailing direction is also affected by the ferry's motion. As the ferry sails, there is a displacement of a large amount of water backwards underneath the hull due to a pressure gradient created by water level differences. However, instead of a backflow, a forward flow is observed in the direction of the ferry's motion and possible origins for its presence are given in this study.

Acknowledgements

I would like to express my deepest gratitude to my supervisor, professor Leo Maas. The completion of this project would not have been possible without his continuous support and guidance. I would also like to extend my thanks to Johan van der Molen and Sjoerd Groeskamp for their assistance and contribution to the project, as well as the support they provided. My collaboration with all three was one of the best experiences I have had through my academic years. Last but not least, I would like to thank my family and friends for their unceasing encouragement and support.

Contents

Chapter 1

Introduction

The Wadden Sea is a coastal wetland consisting of a string of barrier islands and tidal flats that span nearly 500 km along the northern coasts of the Netherlands and Germany, and the North Sea coast of Denmark. The Wadden Sea has attracted many scientists and researchers due to its rich biological diversity and due to the physical processes that take place there such as tides, freshwater discharge, and sediment transport. These processes result in an everchanging morphology of the islands, channels and tidal flats (Wang, 2018; Wang et al., 2012). The Marsdiep inlet, which is located between the mainland of the Netherlands and the island of Texel, is the major tidal inlet connecting the North Sea to the western Dutch Wadden Sea (subfigure (b) in Figure 1.1). Many studies in this area are focused on observing tide-, wind- and density-driven flows, as well as sediment transport (see Section 1.1). This manuscript presents observations of tidal currents obtained with ferry-mounted ADCPs in the Marsdiep tidal inlet. This introductory chapter presents an overview of the research outline of the thesis as well as the study area and its tidal characteristics.

1.1 Research motivation

Acoustic Doppler Current Profilers (ADCPs) are now widely used for measuring the velocity of the fluid over a depth range. In addition to measuring velocity fields, ADCPs are used in other applications including bathymetry measurements and estimation of sediment concentration. An ADCP can collect backscatter intensity data which can provide estimates of the concentration of scattering particles in the study area of the instrument providing information on suspended sediment transport processes (Kostaschuk et al., 2005).

The most common ADCPs are upward-looking and they are anchored to the seafloor. They are used for in situ measurements of waves and currents in the whole water column. The disadvantage of an upward-looking ADCP is that the measurements are restricted to a single point, along with a temporal analysis only. However, in recent years, this disadvantage has been overcome, by the use of downward-looking ADCP mounted underneath a ship. The advantage of using a hull-mounted ADCP is that it introduces spatial variability into the sampling (Neill and Hashemi, 2018). Therefore, the velocity fields can be measured along the whole transect, from which the spatial profile can be constructed, and along a series of transects from which one can plot the temporal evolution of the velocity fields.

For the last two decades, various investigations and studies regarding the physical processes and the geomorphodynamics of the Marsdiep inlet have been conducted. In cooperation with the ferry company Texels Eigen Stoomboot Onderneming (TESO), the Royal Netherlands Institute for Sea Research (NIOZ) has conducted ferry-mounted ADCP measurements in the Marsdiep tidal inlet since 1998. These high-frequency measurements are being taken by an ADCP instrument mounted on a ferry that crosses the inlet multiple times a day. Buijsman and Ridderinkhof, 2007 and Buijsman and Ridderinkhof, 2008 are the first who investigated the tidal currents and the sand waves in the area using the vessel-mounted ADCP data. Moreover, Nauw et al., 2014 managed to determine the volume flux and the flux of suspended particulate matter (SPM). The common feature of those studies was that the ADCP was located at the hull, below the water surface near the horizontal center of the ferry. Two years later, two ADCPs were mounted at the bow and the stern of the TESO ferry. However, Sassi et al., 2016 investigated the residual water transport in the Marsdiep inlet by using only the ADCP that is located at the front of the ferry (in the direction of the ferry's motion) to avoid bubble-induced noise which is generated by the ship's propeller.

Now, in this project, we analyze the timeseries of the transects of the velocity field in the Marsdiep inlet which are extracted by both ADCPs mounted under the bow and the stern of the TESO ferry. This gives us the opportunity to investigate not only the tidal currents which pass through the Marsdiep inlet in the Wadden Sea, but the feature of turbulence as well. In previous years, turbulence characteristics were studied by de Vries, 2015 by using a single upward-looking ADCP mounted at the bottom of the inlet which was measuring the mean and time fluctuating parts of the velocity field. He managed to estimate the turbulent kinetic energy production and dissipation by combining two techniques. He computed the Reynolds' stresses and the turbulent kinetic energy shear production by using the variance method described by Stacey, Monismith, and Burau, 1999 while the turbulent kinetic energy dissipation rate was calculated through the structure function method described by van Haren, Oakey, and Garrett, 1994 (for further details see de Vries, 2015). In this study, by combining the data of those two ADCPs, we manage to extract this turbulence feature as well as its variation with the phase of the tide. Furthermore, despite the fact that the ADCP data is corrected for the ferry's velocity, we speculate that the ferry's motion affects the measurements by physical changes to the velocity field. Therefore, we search for the influence of the ship's motion on the vertical and the along-ship horizontal velocity measurements. This knowledge might lead to correcting the ADCP data which is possibly contaminated by the ship-induced effect. In summary, what we search for in this research study are:

- the tidal characteristics of the flow and evidence of turbulence features in the Marsdiep inlet,
- a correction of the measured vertical velocity for the ferry's motion and a physical interpretation of the vertical velocity field,
- a correction of the measured horizontal velocity in the sailing direction for the ship-induced backflow.

Chapter 2 presents the data of hull-mounted ADCPs and the methodology to process and extract the correct current data from the noise. Additionally, we will present how to correct the backscatter intensity that the ADCPs measure as well as the methodology of the harmonic analysis that is used for the analysis of the tidal cycle. Ferry-ADCPs observations of tidal currents in the Marsdiep inlet and their characteristics are presented in Chapter 3 along with turbulent features that are extracted by combining the results of the two ADCPs. Chapters 4 and 5 are focused on the investigation of the influence of the ferry's motion on the velocity components in the vertical and the sailing direction, respectively, and on a possible correction of the data. Finally, Chapter 6 presents an overview of the main results, an outlook to remaining gaps in our understanding of the estuarine dynamics in the Marsdiep basin as well as some suggestions for further research.

1.2 The Marsdiep tidal inlet - Study area

The Marsdiep inlet is located between Den Helder and the island of Texel (at 52.985°N and 4.785°W) and it is one of the major tidal inlets connecting the North Sea to the western Wadden Sea. The inlet is about 4 km wide and maximally 27m deep where the ferry crosses and up to 50m deep at the location of Helsdeur (subfigure (a) in Figure 1.1) (Elias and van der Spek, 2017). To the west and at the seaward mouth of the Marsdiep inlet, an ebb-tidal delta with its supratidal sand shoal Noorderhaaks is located. Noorderhaaks is northward separated from Texel by the Molengat channel which extends along the Texel coastline. On the southern part of the ebb-tidal delta, the two main channels Schulpengat and Nieuwe Schulpengat, extend along the North-Holland coastline (Elias and van der Spek, 2017). At the basin side of the area, the inlet channel bifurcates in the northern main channel Texelstroom and the southern secondary Malzwin channel. The tidal currents flow through Schulpengat channel into the Marsdiep basin and the Marsdiep basin drains into the North Sea through Molengat channel.

The tidal wave in the Wadden Sea originates from the southern part of the North Sea through the Marsdiep inlet. The tides enter the North Sea from the Atlantic Ocean as a Kelvin wave. The Kelvin wave which propagates southward along the east coast of the United Kingdom meets the Kelvin wave which propagates

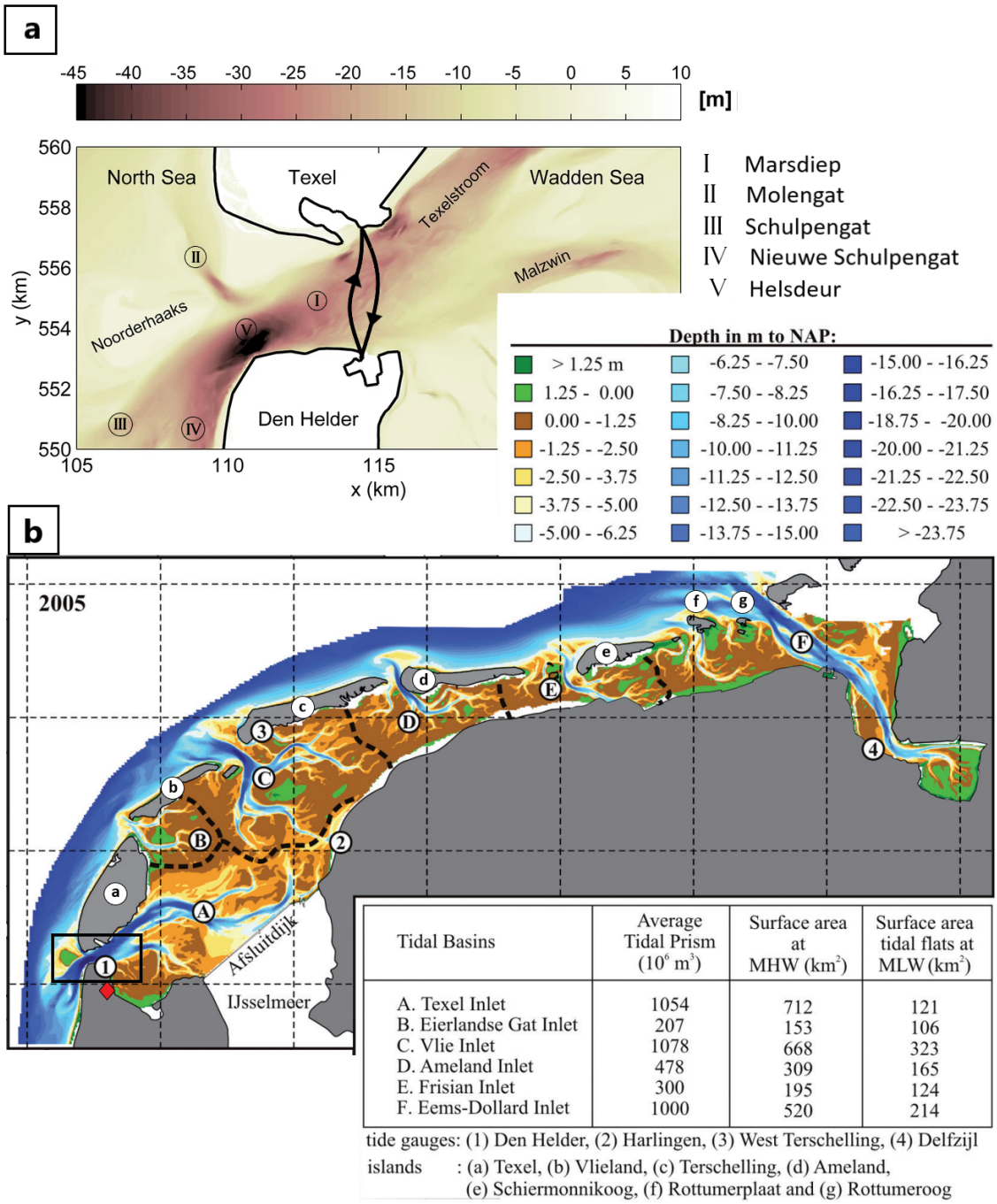

Tidal Basins	Average Tidal Prism (10^6 m^3)	Surface area at MHW (km^2)	Surface area tidal flats at MLW (km^2)
A. Texel Inlet	1054	712	121
B. Eierlandse Gat Inlet	207	153	106
C. Vlie Inlet	1078	668	323
D. Ameland Inlet	478	309	165
E. Frisian Inlet	300	195	124
F. Eems-Dollard Inlet	1000	520	214

tide gauges: (1) Den Helder, (2) Harlingen, (3) West Terschelling, (4) Delfzijl
islands : (a) Texel, (b) Vlieland, (c) Terschelling, (d) Ameland, (e) Schiermonnikoog, (f) Rottumerplaat and (g) Rottumeroog

FIGURE 1.1: The Marsdiep inlet (subfigure (a)) in the western Dutch Wadden Sea (subfigure (b)). Subfigure (b) illustrates the configuration of the inlets, basins, channels and shoals for the year 2005 (adapted from Elias et al., 2012). The Marsdiep tidal inlet is indicated by the black rectangle. The red rhombus indicates the station of the Royal Netherlands Meteorological Institute (KNMI) in De Kooy. Subfigure (a) shows the configuration of the channels in the Marsdiep inlet (adapted from Ponsoni et al., 2019). The two black curves represents the trajectory of the ferry's crossings. In both figures, the colored contours represent the bathymetry (elevation from the seabed) in m.

through the Dover Strait, between United Kingdom and France. These two Kelvin waves interfere among them and are distorted due to the Coriolis effect and bottom friction. As a result, a complicated tidal wave pattern is created. The semi-diurnal tidal wave rotates counterclockwise around two amphidromic points, one located in the southern North Sea between the Netherlands and the United Kingdom and one to the west of Denmark. The tide propagates northward, along the Dutch coasts and finally enters the Marsdiep channel from the south near Den Helder and propagates northward towards Texel and eastward into the inlet (Elias, Pearson, and van der Spek, 2020; Buijsman, 2007).

The currents in the Marsdiep inlet are governed by the semi-diurnal tides. The most dominant tide in the inlet is the semi-diurnal lunar tide (M2 tide) that has a period of about 12 hours and 25.2 minutes, while the second largest constituent ($\sim 27\%$ of M2) is the semi-diurnal solar tide (S2 tide) with a 12 hour period. The interaction between the M2 and S2 constituents results in the spring-neap cycle (de Vries, 2015; Buijsman and Ridderinkhof, 2007). Also, another important compound and overtide in the inlet is the M4 shallow-water constituent. Due to the interaction of the M2 and M4 constituents, a tidal asymmetry is observed in the Marsdiep inlet. Specifically, during a flood the largest velocities are equally distributed across the inlet with small tidal residual flow close to the Den Helder coastline whereas during an ebb there is a large ebb-dominant flow in the northern half of the inlet (Elias and van der Spek, 2017; Nauw et al., 2014).

Chapter 2

Data and Methods

In this chapter we focus on the presentation of the hull-mounted ADCPs data obtained in the period 2020-2022 and the methodology of obtaining this data. In addition, a short description on discarding the bad quality data is given. Moreover, the following section in this chapter presents the method used for converting the backscatter intensity that the ADCPs measure from counts to decibels as well as for the backscatter intensity correction due to fluid attenuation. Finally, the last section of this chapter presents the methodology of the least-squares harmonic analysis. The harmonic analysis provides the contribution of the tidal constituents to the tidal cycle.

2.1 Data collection

This research project is based on current measurements from a ferry on each transect across the Marsdiep inlet. A company named Texels Eigen Stoomboot Onderneming (TESO) has been offering the ferry service between Texel and Den Helder. The ferry has 135.4m length, 27.9m max breadth, 23m breath hull and 4.4m max draft (Trauthwein, October 2019). The current velocity profile is measured with two four-beam 1.2MHz RDI Workhorse Monitor ADCPs mounted on the ferry. The two ADCPs are mounted underneath the hull at 4.4 m below the water surface, toward the bow and the stern of the ferry as illustrated in Figure 2.1. The two ADCPs have a blanking distance of 1m resulting in a coverage from 5.4m beneath the sea surface to the bottom with a vertical resolution of 0.5m and a sampling period of 1s (one ping per ensemble of one second). Therefore, if the ferry's speed is around 5 m/s then the distance between two subsequent measurements is 5m. The TESO ferry crosses the Marsdiep inlet between the harbours of Den Helder and Texel every 30 min on a daily basis from about 06:00 to 22:00, up to 32 times per day. The duration of the crossings varies between 15 and 20 minutes (Sassi et al., 2016). The ferry sails up and down without reversing. Therefore, in order to distinguish the two ADCPs, the ADCP which is placed on the side of the Texel is denoted *tx*, while the other one which is placed on the side of the Den Helder is denoted *hd*. While the ferry sails across the inlet, the ADCP data are stored and at night, when the ferry docks at Texel, the data are automatically transferred by telemetry to a computer at NIOZ for further processing.

Each measurement collected by the ADCP consists of the following data: date and time; latitude and longitude coordinates; depth of the measurement; zonal, meridional and vertical water velocities as measured by the ADCP apparatus; the bottom track velocity; the ferry's GPS velocity; the ferry's heading, pitch and roll and as well the acoustic intensity of back reflected sound (echo intensity) and an error velocity ε. An ADCP with four transducers allows for measuring two horizontal velocities as well as two times the vertical velocity. One pair of beams obtains one horizontal component and the vertical velocity component. The second pair of beams obtain a second, perpendicular horizontal component as well as a second vertical velocity component. Thus, a four beam ADCP measures two horizontal velocity components and two vertical velocity components. The average of the two vertical components is the vertical velocity and the difference between these two vertical velocities is defined as error velocity and it is used as a measure of accuracy (Soons, 2022; Teledyne RD Instruments, 2011; Gilcoto, Jones, and Fariña-Busto, 2009).

The velocity data are retrieved in beam coordinates. Therefore it must be corrected for the ferry's motion and transformed to geographic coordinates (Sassi et al., 2016). Differential global positioning system (DGPS) and gyrocompass as well as bottom track (BT) system were used to determine the ferry's location,

FIGURE 2.1: The TESO ferry sails in the Marsdiep inlet, between Texel and Den Helder. Two ADCPs are mounted underneath the hull below the water surface, toward the bow and the stern of the ferry. The ADCP which is placed on the side of the Texel is denoted *tx*, while the other one which is placed on the side of the Den Helder is denoted *hd*. The figure is retrieved from the website of the Royal Netherlands Institute for Sea Research (link:`https://www.nioz.nl/en/expertise/wadden-delta-research-centre/facilities-technology/instruments/dynamics-of-the-marsdiep`).

orientation and speed. The flow profiles are corrected for vessel motion by using the bottom-track velocity. In the case that the bottom-track velocity is unavailable, then the velocity measured by the GPS is used. The corrected flow's velocity data are hence: the eastward (u), northward (v) and vertical (w) in geographic coordinates. Velocity directed to the east (west) and into (out of) the Wadden Sea is positive (negative). Velocity directed to the north (south) towards Texel (Den Helder) is positive (negative), while the positive (negative) vertical velocity corresponds to the upward (downward) motion of the flow.

The data was collected during a series of measurements from January 2020 to June 2022. The measurements were carried out during a semi-diurnal tidal cycle along different ferry's crossings. In addition to the ferry data, 10 min water-level data measured at the Den Helder port, were obtained from the Dutch Ministry of Infrastructure and Water Management.

2.2 Quality of ADCP data

During the crossings, sometimes, poor-quality ADCP data was collected. The data which is extracted by the ADCP located on the stern of the ferry (depending on the direction of the ferry), especially, is noisy due to air bubbles produced by the wake of the ferry propulsion (Sassi et al., 2016). In Figure 2.2, an example of a vertical profile of the eastward velocity along the Marsdiep inlet is given. The data was extracted on August 11, 2020, during the 14th crossing of the TESO ferry. As the ferry sails from Texel to Den Helder, the *tx* ADCP, located at the rear of the ferry, records some bad quality data (subplot (c)) which is depicted with dark red and blue color in the middle of the transect. This bad data can be screened out by adjusting a velocity threshold which corresponds to the error velocity. If the ADCP raw data exceeds the specified threshold, the particular data is flagged as bad, presented with empty bins (subplot (d)) and not considered in the computations (Meteorological Service of Canada, 2004). If more than a set proportion of the water column is flagged, then the whole column gets flagged. By lowering this velocity threshold, more data is flagged as bad and consequently larger number of empty bins appear in the velocity contours. The values of the velocity threshold that were used in the analysis were chosen between the range 0.2 and 0.4 m/s.

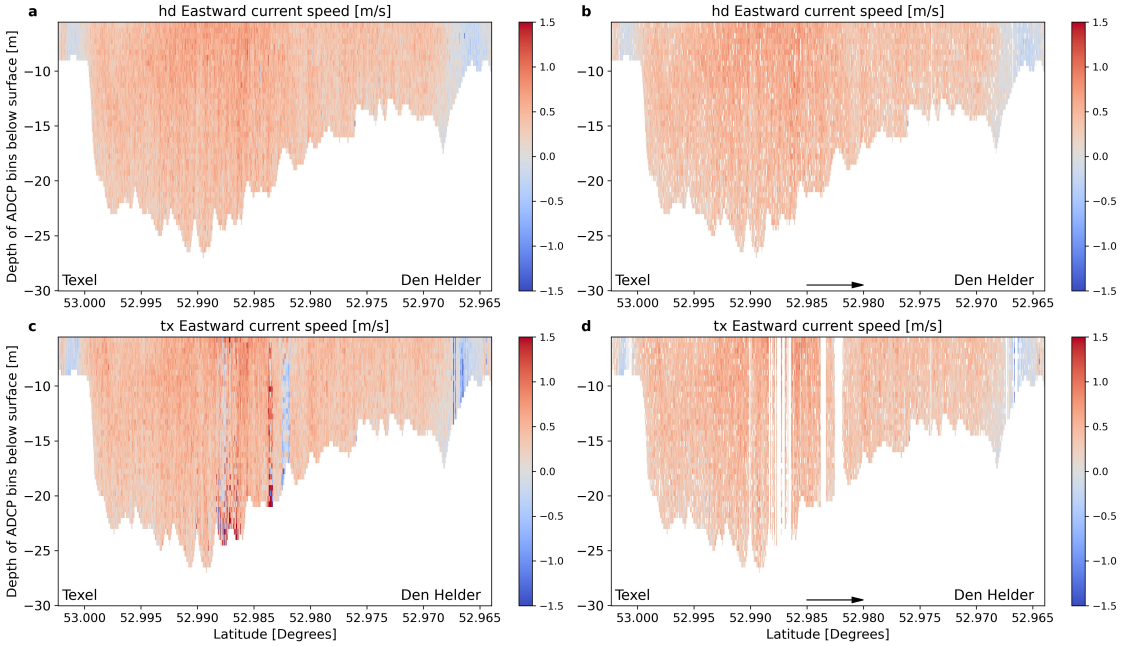

FIGURE 2.2: Vertical profile of the eastward water velocity that the two ADCPs measured separately across the Marsdiep inlet on August 11, 2020. During the 14th crossing the ferry sails from Texel to Den Helder as the black arrow near the bottom of the right panels notates. Subplots (a) and (c) present the raw data for the *hd* (front) ADCP and the *tx* (rear) ADCP respectively. Subplots (b) and (d) present the data in which the bad data was removed and it is replaced by empty bins for the *hd* ADCP and *tx* ADCP respectively.

2.3 Echo intensity

The ADCP also receives the intensity of the sound wave which is reflected from an object back to the transducer. Commercially available ADCPs report a measure of backscatter as the echo intensity (EI), in counts, which is converted to backscatter in decibels by the relation (Haught, Venditti, and Wright, 2017):

$$I_{db} = k_c(EI - NL) \tag{2.1}$$

where NL is the noise level in counts. For 600 and 1200kHz RD Instruments Workhorse or Broadband ADCP, a typical value for the noise level is 40 counts (Deines, 1999). The variable k_c (= 0.43 dB/count) is the received signal strength indicator scale factor and it is a temperature-dependent instrument constant.

Then, the backscatter intensity should be corrected for transmission losses due to geometrical spreading and fluid attenuation. With this correction, the backscatter intensity is converted to a physical signal which in turn can be converted into a sediment concentration. The fluid corrected backscatter (I_{FCB}) is computed in dB by the equation (Haught, Venditti, and Wright, 2017):

$$I_{FCB} = I_{db} + 20\log(R) + 2\alpha_f R \tag{2.2}$$

where α_f is the fluid attenuation and R is defined as (Ghaffari et al., 2011; Deines, 1999):

$$R = \frac{z}{\cos(\theta)} + \frac{D}{4} \tag{2.3}$$

where θ (= 20°) is the angle beam, D (= 0.5m) is the bin size and z is the bin depth.

The second term on the right-hand side of eq. (2.2) is linked to the beam's spherical spreading and the third term accounts for fluid attenuation. The fluid attenuation coefficient α_f [dB/m], is the sum of relaxation due to a boric acid component, a magnesium sulphate component and a viscosity component[1], which can be written as (Aardoom and Mol, 2006; Medwin and Clay, 1998):

$$\alpha_f = \left[\frac{A_1 P_1 f_1 f^2}{f^2 + f_1^2} + \frac{A_2 P_2 f_2 f^2}{f^2 + f_2^2} + A_3 P_3 f^2\right] \cdot 10^{-3} \tag{2.4}$$

for the boric acid component:

$$A_1 = \frac{8.68}{c} 10^{(0.78pH-5)} \qquad [dB\ km^{-1}\ kHz^{-1}]$$
$$P_1 = 1$$
$$f_1 = 2.8\sqrt{\frac{S}{35}}\ 10^{[4-1245/(273+T)]} \qquad [kHz]$$

for the magnesium sulphate component:

$$A_2 = 21.44\frac{S}{c}(1+0.025T) \qquad [dB\ km^{-1}\ kHz^{-1}]$$
$$P_2 = 1 - 1.37\cdot 10^{-4} z + 6.2\cdot 10^{-9} z^2$$
$$f_2 = \frac{8.17\cdot 10^{[8-1990/(273+T)]}}{1+0.0018(S-35)} \qquad [kHz]$$

and the viscosity component:

$$A_3 = 4.937\cdot 10^{-4} - 2.59\cdot 10^{-5} T + 9.11\cdot 10^{-7} T^2 - 1.5\cdot 10^{-8} T^3 \quad \text{if T} \leq 20^{\circ}\text{C}$$
$$A_3 = 3.964\cdot 10^{-4} - 1.146\cdot 10^{-5} T + 1.45\cdot 10^{-7} T^2 - 6.5\cdot 10^{-8} T^3 \quad \text{if T} > 20^{\circ}\text{C}$$
$$[dB\ km^{-1}\ kHz^{-2}]$$
$$P_3 = 1 - 3.83\cdot 10^{-5} z + 4.9\cdot 10^{-10} z^2$$

where f is the ADCP's working frequency (=1200 kHz), pH denotes the acid degree (= 8.1), S is salinity (= 28 psu), T is the average water column temperature (=15.5°C) and c is the speed of sound [m/s] given by:

$$c = 1449.2 + 4.6T - 0.055T^2 + 0.00029T^3 + (0.0134T)(S-35) + 0.016z$$

According to Haught, Venditti, and Wright, 2017, eq. (2.2) is valid at low sediment concentrations, where sediment attenuation is much smaller than the fluid attenuation. For higher concentration, attenuation increases and it is necessary to correct acoustic backscatter for sediment attenuation as well. Therefore, to account for two-way transmission losses associated with the viscous and scattering effects of sediment, the sediment corrected backscatter (I_{SCB}) is computed as (Haught, Venditti, and Wright, 2017):

$$I_{SCB} = I_{FCB} + 2\alpha_s R \tag{2.5}$$

The sediment attenuation coefficient α_s, can be estimated either theoretically or in situ. However, the in situ estimates are more efficient to be used because the theoretical estimates of sediment attenuation require a priori knowledge of the sediment concentration and grain-size distribution (Haught, Venditti, and Wright, 2017). In this study, only the fluid corrected backscatter is used.

[1] As the sound wave travels thought the sea, the molecules of the water start vibrating. For frequencies above 100 kHz, the vibration of the water particles produces thermal energy by viscous drag. For frequencies below 100 kHz, chemical components such as magnesium sulfate (>10 and <100 kHz) and boric acid (<10 kHz) dissociate, producing thermal energy (Doonan, Coombs, and McClatchie, 2003).

2.4 Harmonic analysis

Harmonic analysis is a mathematical tool, used for the representation of signals as the superposition of basic waves and it is used to explain the variations in the timeseries of the measured velocity dataset by using the least squares method. This timeseries of the velocity is a combination of known astronomical tidal constituents. A single frequency, phase and amplitude correspond to each tidal constituent. The harmonic analysis will be used on the timeseries of the northward velocity in Chapter 5 to investigate the ferry's induced effect in the sailing direction. After the implementation of the least squares method on the dataset, we obtain the best harmonic fit of the timeseries; the explained timeseries.

By using harmonic analysis, we obtain the minimum difference between the measured and the fitted (explained) data. This difference between the measured and the explained timeseries is called residual timeseries:

$$v_i^{res} = v_i^{meas} - v_i^{fit} \tag{2.6}$$

where v_i^{res} is the residual velocity, v_i^{meas} is the measured velocity and v_i^{fit} is the best fitted velocity. The index i represents a discrete time which total to N, the total number of data points. The residual velocity becomes smaller as the fitting of the harmonic analysis is improved. The explained variation is defined as a sum of harmonic components with known astronomical tidal frequencies. During this study the sum consists solely of cosines and sines at the M2, M4, M6 and M8 tidal frequencies as follows:

$$v_i^{fit} = B_0 + \sum_{m=1}^{M} [B_m \cos(\omega_m t_i) + C_m \sin(\omega_m t_i)] \tag{2.7}$$

where $m = 1,2,..,M$, M is the number of tidal frequencies, B_0 is the off-set, B_m and C_m are the amplitudes of the tidal constituents, ω_m is the tidal frequency, and t_i is the time that corresponds to the i-th fitted measurement.

The residual velocity corresponds to the variations that are not explained by these four tidal constituents. Some examples are wind- and density-driven current variations, turbulence and instrument noise as well as other harmonic constitutes not included in this analysis. The residual velocity is defined as the function of the sum of squared errors (SSE) (Maas, 2019; Groeskamp, 2008):

$$SSE = \sum_{i=1}^{N} (v_i^{res})^2 = \sum_{i=1}^{N} (v_i^{meas} - v_i^{fit})^2 \tag{2.8}$$

By minimizing this variable, we can find amplitudes B_0, B_m and C_m. This minimum is obtained when all the partial derivatives of the amplitudes vanish ($\partial_{B_0} SSE$, $\partial_{B_m} SSE$, $\partial_{C_m} SSE$) = 0. The nine set of equations which arise with the minimization can be rewritten into matrix form as:

$$AX = M \tag{2.9}$$

where

$$A = \begin{pmatrix} N & c_1 & s_1 & c_2 & s_2 & c_3 & s_3 & c_4 & s_4 \\ c_1 & c_1c_1 & c_1s_1 & c_1c_2 & c_1s_2 & c_1c_3 & c_1s_3 & c_1c_4 & c_1s_4 \\ s_1 & s_1c_1 & s_1s_1 & s_1c_2 & s_1s_2 & s_1c_3 & s_1s_3 & s_1c_4 & s_1s_4 \\ c_2 & c_2c_1 & c_2s_1 & c_2c_2 & c_2s_2 & c_2c_3 & c_2s_3 & c_2c_4 & c_2s_4 \\ s_2 & s_2c_1 & s_2s_1 & s_2c_2 & s_2s_2 & s_2c_3 & s_2s_3 & s_2c_4 & s_2s_4 \\ c_3 & c_3c_1 & c_3s_1 & c_3c_2 & c_3s_2 & c_3c_3 & c_3s_3 & c_3c_4 & c_3s_4 \\ s_3 & s_3c_1 & s_3s_1 & s_3c_2 & s_3s_2 & s_3c_3 & s_3s_3 & s_3c_4 & s_3s_4 \\ c_4 & c_4c_1 & c_4s_1 & c_4c_2 & c_4s_2 & c_4c_3 & c_4s_3 & c_4c_4 & c_4s_4 \\ s_4 & s_4c_1 & s_4s_1 & s_4c_2 & s_4s_2 & s_4c_3 & s_4s_3 & s_4c_4 & s_4s_4 \end{pmatrix} \tag{2.10}$$

and

$$M = \begin{pmatrix} \sum_{i=1}^{N} v_i^{meas} \\ c_1 \sum_{j=1}^{N} v_j^{meas} \delta_{ij} \\ s_1 \sum_{j=1}^{N} v_j^{meas} \delta_{ij} \\ \vdots \\ c_4 \sum_{j=1}^{N} v_j^{meas} \delta_{ij} \\ s_4 \sum_{j=1}^{N} v_j^{meas} \delta_{ij} \end{pmatrix} \tag{2.11}$$

where we abbreviate

$$c_x = \sum_{i=1}^{N} \cos(xt_i) , \qquad s_x = \sum_{i=1}^{N} \sin(xt_i) \tag{2.12}$$

and

$$c_x c_y = \sum_{i=1}^{N} \cos(xt_i)\cos(yt_i) \tag{2.13}$$

$$s_x s_y = \sum_{i=1}^{N} \sin(xt_i)\sin(yt_i) \tag{2.14}$$

$$c_x s_y = \sum_{i=1}^{N} \cos(xt_i)\sin(yt_i) \tag{2.15}$$

where $x, y = \omega_m$ (where $m = 1,2,3,4$). The elements of the matrix X are unknown and they correspond to the amplitudes of the tidal constituent.

$$X = \begin{pmatrix} B_0 \\ B_1 \\ C_1 \\ \vdots \\ B_4 \\ C_4 \end{pmatrix} \tag{2.16}$$

Therefore, the unknown best fit amplitudes can be found via inversion of matrix A:

$$X = A^{-1}M \tag{2.17}$$

Chapter 3

Ferry-ADCP observations of tidal currents and tidally induced turbulence

The abundance of available data allows us to investigate the spatial and temporal variability of the velocity field of the flow. In this chapter, this data is presented. Also, we try to identify physical characteristics of the tides in the Marsdiep inlet which are referred to in the literature as the phase difference between the water elevation and the tidal current. Furthermore, we would like to exploit the fact that two ADCPs are mounted on the ferry. One can say that the ADCPs should measure the same velocity field of the flow after the implementation of the quality control. In this chapter, we see that the results of the two ADCPs are not identical but they differ slightly. We investigate whether the origin of this difference is instrumental or physical. More specifically, we search for evidence for tidally induced turbulence by combining the ADCPs results.

3.1 Introduction

The Marsdiep inlet is governed by two different water masses; the freshwater discharged from the Lake IJssel and the saline water from the North Sea. The exchange of the water masses between the Marsdiep basin and the North Sea primarily occurs due to the semi-diurnal tides. More specifically, the freshwater transports from Texelstroom and Malzwin channels into the North Sea as an ebb southwesterly outflow. As time passes, the flood current begins entering the inlet along the coast of Den Helder but due to tidal asymmetry the centre of the inlet is dominated by the ebb current. Then the ebb flow weakens and strong flood velocities get distributed along the inlet (Elias and van der Spek, 2017; Buijsman, 2007). In the next section we search for this tidal asymmetry (due to interaction of M2 and M4 tides) along the transect by using the ADCP measurements. Moreover, the semi-diurnal tidal waves in the inlet are both partially progressive and standing and this can be found by computing the phase difference between the strength of the tidal current and the height of the sea surface.

Another important feature in the Marsdiep inlet, which plays a crucial part in natural systems is the tidally induced turbulence. Turbulence determines the vertical structure of the flow's velocity as well as the vertical distribution of suspended matter. In the Marsdiep basin, the origin of turbulence is assumed to be the velocity's shear close to the bottom of the sea, which is generated by bed friction. This velocity's shear varies between the tidal currents leading to different dynamics during ebb and flood (de Vries, 2015). So far, the turbulent features in the Marsdiep inlet were studied by using in situ datasets (de Vries, 2015). In this study, we are looking for evidence of turbulence along a transect by combining the results of the two ADCPs.

3.2 Results and Discussion

3.2.1 Spatial distribution of tidal currents

Figure 3.1 shows the profile of the eastward (left column) and the northward velocity (right column) measurements along the inlet extracted by the ADCP which is located underneath the hull at the front of the ferry during three different crossings (6th, 18th and 28th crossings) on July 15, 2021. During these transects we observe three different tidal currents; flood current (top row), ebb current (middle row) and slack current (bottom row). Regarding the strength of the tides, the eastward velocity peaks at around 1.4 m/s whereas the northward velocity peaks at around 1.0 m/s. It is important to note that, these maximum values, slightly vary from day to day, but the eastward velocity peak is always larger than the absolute value of the northward one. Furthermore, we observe that the flood current is more uniformly distributed along the inlet compared to the ebb current. Simply put, the strongest flood currents occur along the transect whereas the largest ebb currents occur close to the Texel coastline. According to the literature, this tidal asymmetry causes a counterclockwise horizontal residual circulation cell with a small floodward residual currents along the

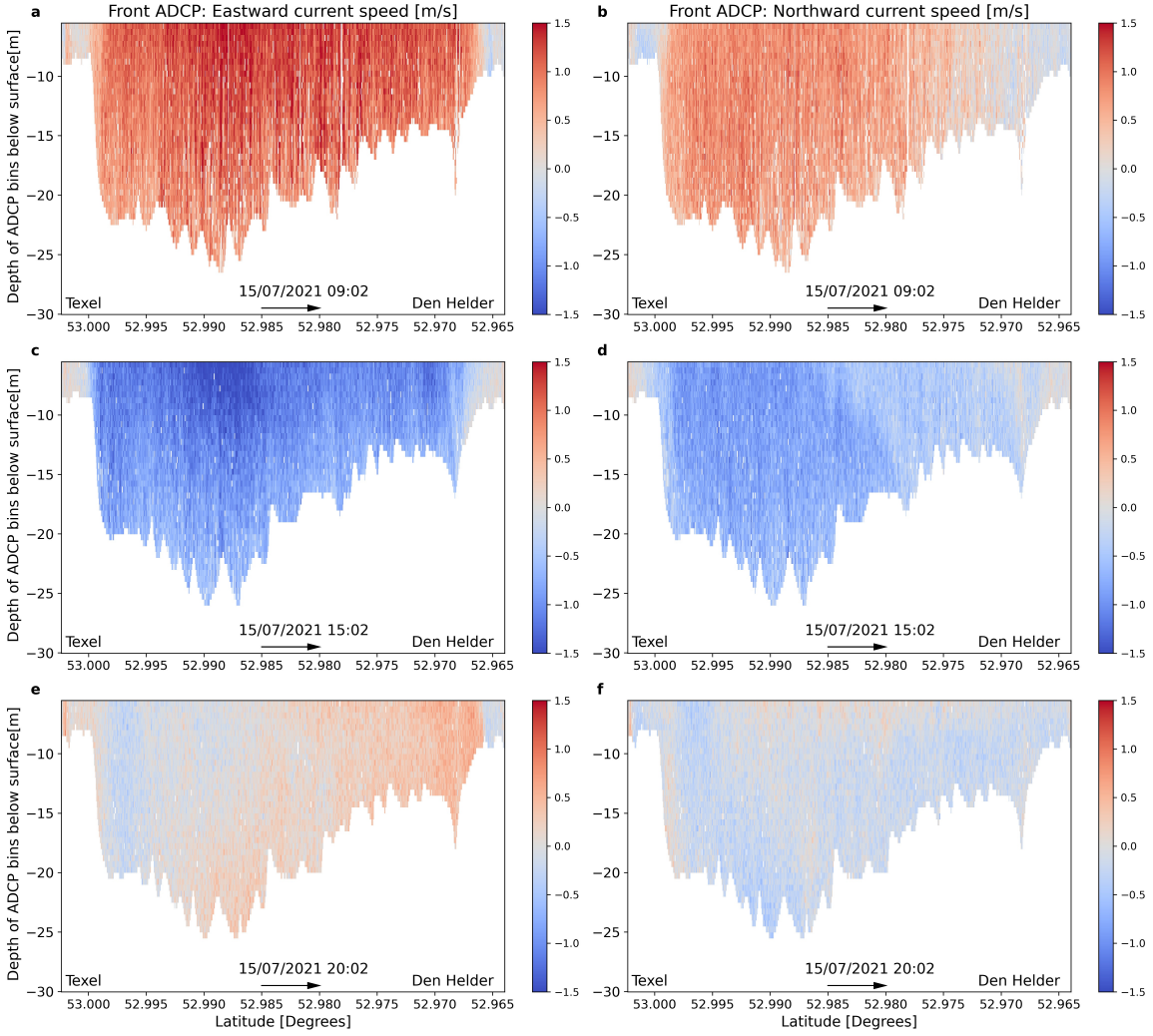

FIGURE 3.1: Profiles of the eastward (left column) and northward (right column) velocity of the flow across the Marsdiep inlet during three different crossings of the ferry from Texel to Den Helder as measured by the ADCP which is located underneath the hull at the front of the ferry on July 15, 2021. Subplots (a) and (b) correspond to a flood current, subplots (c) and (d) correspond to an ebb current and subplots (e) and (f) correspond to a slack current.

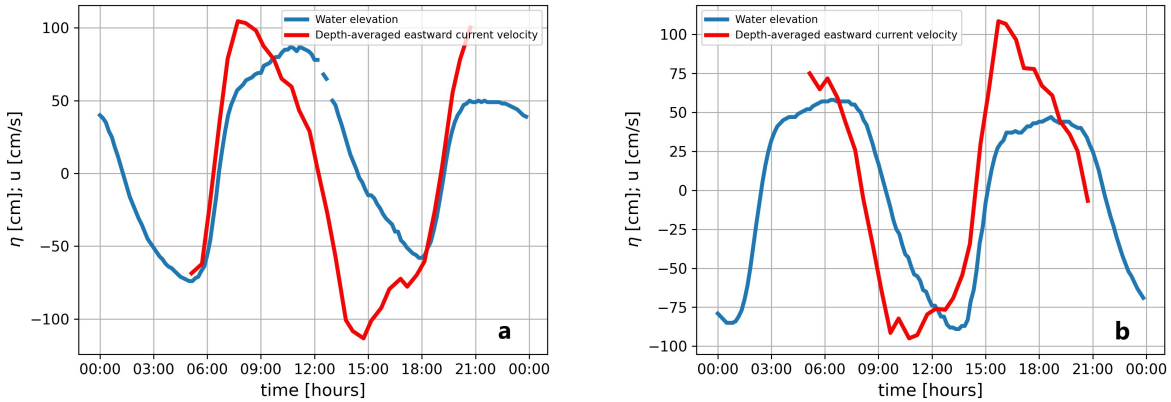

FIGURE 3.2: Time series of water elevation and the eastward tidal current in the Marsdiep inlet during a spring tide on July 15, 2021 (subplot(a)), and during a neap tide on July 23, 2021 (subplot (b)). The hours of the day are shown in CET time zone.

Den Helder coastline and large ebbward residual currents along the Texel coastline (Elias and van der Spek, 2017; Buijsman, 2007). This feature is also apparent in the slack current where there is a flood-dominant current in the southern and ebb-dominant current in the northern side of the inlet.

3.2.2 Phase lag between water elevation and tidal current

The timeseries of the water elevation (η) recorded at Den Helder's ferry port during a spring tide on July 15, 2021, and during a neap tide on July 23, 2021, are shown in Figure 3.2. On the same figures, the time-series of the eastward tidal current are illustrated. The tidal current is calculated by averaging the eastward velocity, which is measured by the two ADCPs, over the water depth at a specific location (52.9883°N) in the Marsdiep inlet. For this calculation, the water velocity data is binned in 100 equidistant intervals across the transect in an attempt to reduce the noise. A positive tidal current which is directed into the Wadden Sea is associated with a flood current, whereas a negative tidal current which is directed out of the Wadden Sea is associated with an ebb current. By looking at the two curves, a phase difference between the water elevation and the tidal current is observed. The time difference between the curves is approximately found equal to 2 - 2.5 hours. This lag indicates whether the tidal wave in the Marsdiep channel is progressive or standing. According to the theory, the phase lags of 0° and 90° correspond to progressive[1] and standing[2] waves, respectively (Khojasteh et al., 2020; Ward et al., 2018). In the case that phase lag lies between these two values, the waves are mixed. In the Marsdiep tidal inlet, there is a phase lag of 59-73° between the water level and the tidal current, indicating that the semi-diurnal tidal waves are both partially progressive and standing. This mixture between a standing wave and progressive wave can be explained due to the reflection of the incoming tidal wave, through the Marsdiep inlet, at the end of the Wadden Sea basin (Groeskamp, 2008).

Figure 3.2 also reveals an asymmetry in the maximum velocities and the duration of the flood and ebb phase. The flood current is stronger than the ebb current, whereas the duration of the ebb phase is longer than that of the flood's. According to Guo et al., 2019, these differences are caused due to the phase difference between the M2 and M4 tidal constituents in the inlet. However, this tidal asymmetry differs between the spring and the neap tide. During spring tides, the curve of the current is skewed whereas during the neap tides the curve is symmetrical. Furthermore, the duration of the flood period during spring tides is shorter than during neap tides. This difference between the spring and the neap tides as well as further study on the tidal asymmetry is discussed in Guo et al., 2019.

[1] when peak tidal currents occur at high and low tide

[2] when peak tidal currents occur midway between high and low tide

3.2.3 Tidally induced turbulence

In this section we compare the horizontal velocities (eastward and northward) at each measured latitudinal location with an average time difference between the measurements of the two ADCPs of 30s. Note that the ferry does not sail in a straight line (subfigure (a) in Figure 1.1) and its speed changes along its trip and as a result the two ADCPs do not take the velocity measurements at exactly the same latitudinal location but it differs by 0.25%. The horizontal velocities are not identical. The difference of the horizontal velocities that were measured from the *hd* and *tx* ADCPs across the Marsdiep inlet on July 15, 2021 during the 28th transect, are calculated, binned and shown in Figure 3.3. These differences are normally distributed around -0.006 and 0.021 m/s with standard deviations 0.197 and 0.209 m/s for the eastward and northward direction. This normal distribution denotes signal noise. Two possible sources of this noise are the instrument's error and turbulence.

If the source of this noise is entirely caused by the instrument's error, then we expect that the standard deviation of the normal distribution of the horizontal velocities' differences will be constant for any transect. Otherwise, if this standard deviation varies among the transects, then this might be evidence that turbulence is present. Therefore, the normal distributions of the noise, for the 32 transects of the day for 6 days (from July 19 to July 24, 2021) were studied. The standard deviation of those distributions are plotted as a function of the tidal current, which is averaged across the inlet (excluding the harbors by using the data which lies between the 52.967°N and 52.999°N latitude) and depths (excluding the first 10m to reduce the chance to observe artificial turbulence due to ferry's motion), and shown in Figure 3.4. Subplot (a) shows the result for the eastward direction while subplot (b) shows the result for the northward direction. We observe that the standard deviation of the noise varies between 0.20 and 0.28 m/s and it increases for stronger tidal currents. More specifically, the noise is slightly larger during flood currents than ebb currents. We fit the data to identify their correlation and we find a quadratic relation between these two variables of the form $f(x) = ax^2 + k$. $(0,k)$ is the vertex and a represents the concaveness of the parabola. The flood and ebb currents are represented by different quadratic relations. The noise-flood current relation has a lower vertex and sharper concaveness than that of the noise-ebb current relation. Consequently, the noise of the

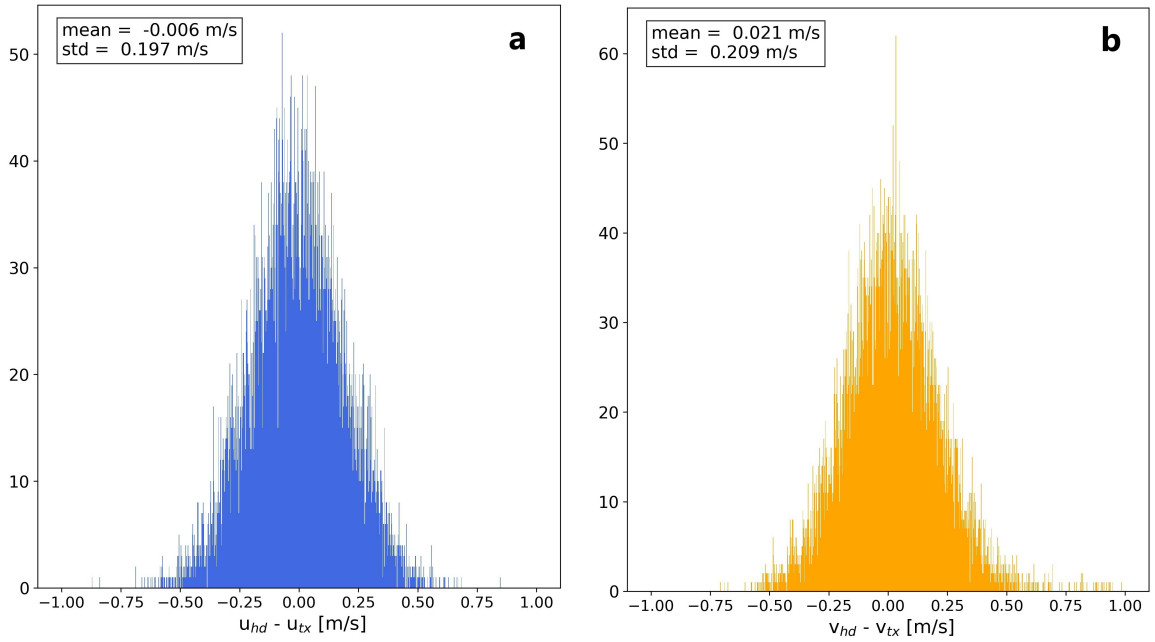

FIGURE 3.3: Normal distributions of the horizontal water velocities' differences measured by the two ADCPs on July 15, 2021, during the 28th crossing of the ferry. Subplot (a) corresponds to the distribution of the difference of the eastward velocities ($u_{hd} - u_{tx}$) while subplot (b) correspond to the difference of the northward velocities ($v_{hd} - v_{tx}$).

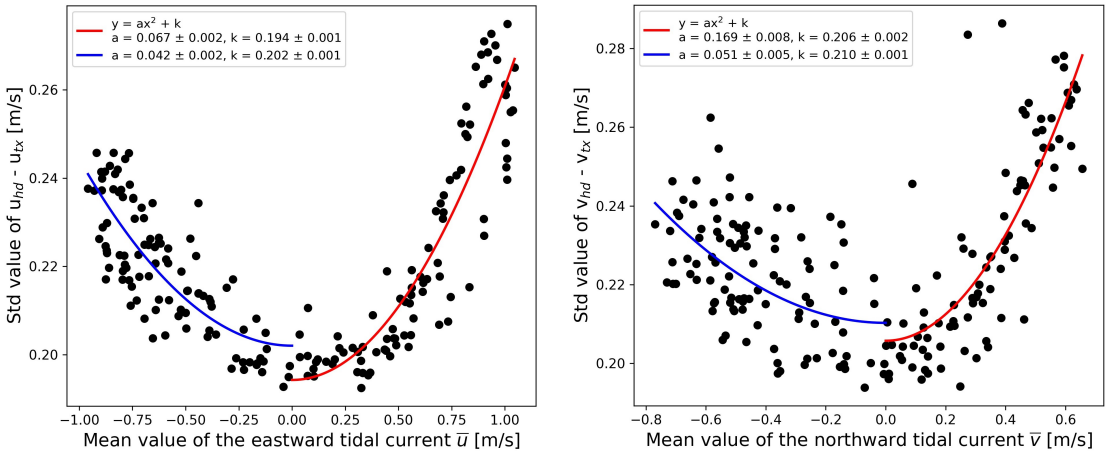

FIGURE 3.4: Standard deviation of the horizontal velocities' difference between the two ADCPs as function of the tidal current, which is averaged across the inlet and depths, for the 32 transects of the day for 6 days (from July 19 to July 24, 2021). Subplot (a) corresponds to difference of the eastward velocities ($u_{hd} - u_{tx}$) while subplot (b) corresponds to the difference of the northward velocities ($v_{hd} - v_{tx}$). The blue line represents the fitted line between the standard deviation of the difference of the horizontal velocities and the ebb current while the red line represents the fitted line between the standard deviation of the difference of the horizontal velocities and the flood current.

measurements of the horizontal velocities varies with the tidal currents, indicating the presence of tidally induced turbulence in the Marsdiep inlet. A method to separate the contribution of turbulence from the noise is not yet found. However, there is a speculation that the instrumental noise level might lie on the vertex, at around 0.2 m/s, and that tidally induced turbulence further raises the value of this standard deviation above 0.2 m/s.

Moreover, the fact that the tidally induced turbulence differs between the flood and the ebb currents is associated with their strength. As we already mentioned, the flood current is stronger than the ebb current. The strength of the tides is proportional to the shear effect of the horizontal velocities in the vertical direction which is responsible for the creation of turbulence (Groeskamp, 2008). The shear is associated with a decrease in magnitude of the horizontal current with depth due to bottom friction. Therefore, this explains the fact that the tidally induced turbulence reaches larger values during the flood current. The tidally induced turbulence and its characteristics will be discussed in detail in the next section.

3.2.3.1 Variations of the tidally induced turbulence depending on the tide's phase

A clear indication that turbulence is related to the strength of the tides is already found. However, by looking at the details of Figure 3.4 , we manage to extract information about the relation between turbulence and the phase of the tide. The tidal current is divided into four phases: the accelerating and the decelerating phase of the flood and ebb currents. These four phases for the eastward and the northward tidal current are illustrated with different colors in subplots (b) of Figures 3.5 and 3.6 respectively. Subplots (a) of those figures show the parabolic relation between the strength of the tides and the tidally induced turbulence (similar to Figure 3.4) with each of the four phases depicted with a different colour. By looking at Figure 3.5, we observe that the magnitude of the tidally induced turbulence increases during the accelerating phase of the flood current. Just after the maximum flood current, the magnitude of turbulence increases further whereas it sharply decreases as the flood current weakens. Similar behaviour is observed during the ebb current. This turbulence seems to vary with the strength of the tides with a pattern in the shape of a butterfly. Therefore, the tidally induced turbulence depends on the phase of the tide indicating that the tidal currents are carrying different amount of turbulence depending on where they come from. The most important characteristics are the following. Firstly the maximum magnitudes of the turbulence are observed just after the maximum

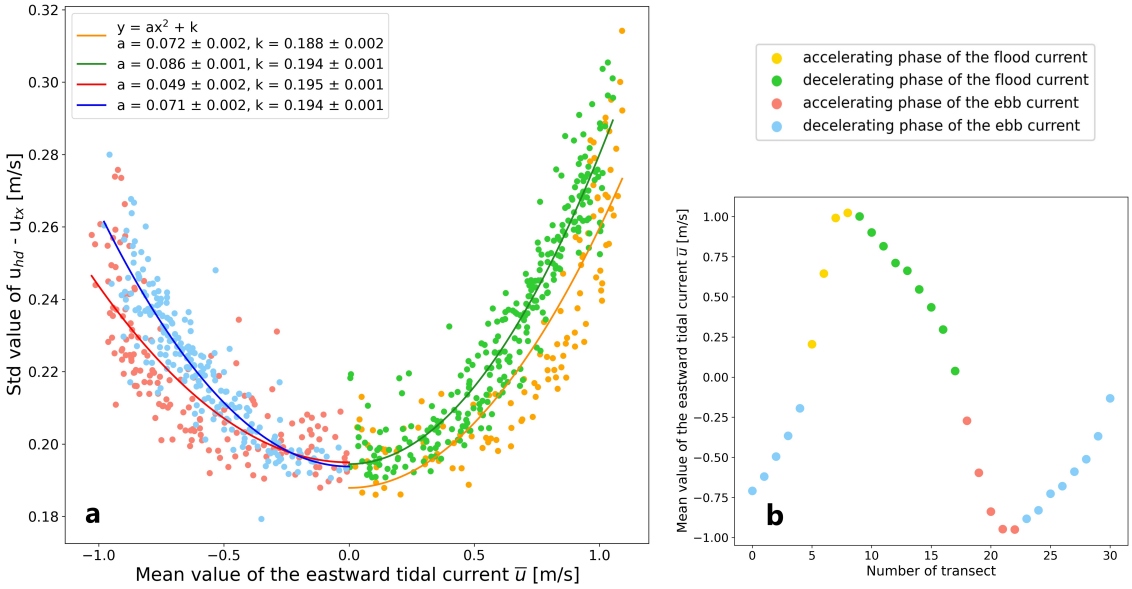

FIGURE 3.5: Subplot (a) corresponds to the standard deviation of the eastward velocities' difference between the two ADCPs as a function of the magnitude of the tidal current, which is averaged across the inlet and depths, for the 32 transects of one month (July 2021). Subplot (b) illustrates the four phases of the eastward tidal cycle. The four phases are represented by different colors of the scatters. The different colored lines represent the fitted lines between the standard deviation of the difference of the eastward velocities and tidal currents for each phase.

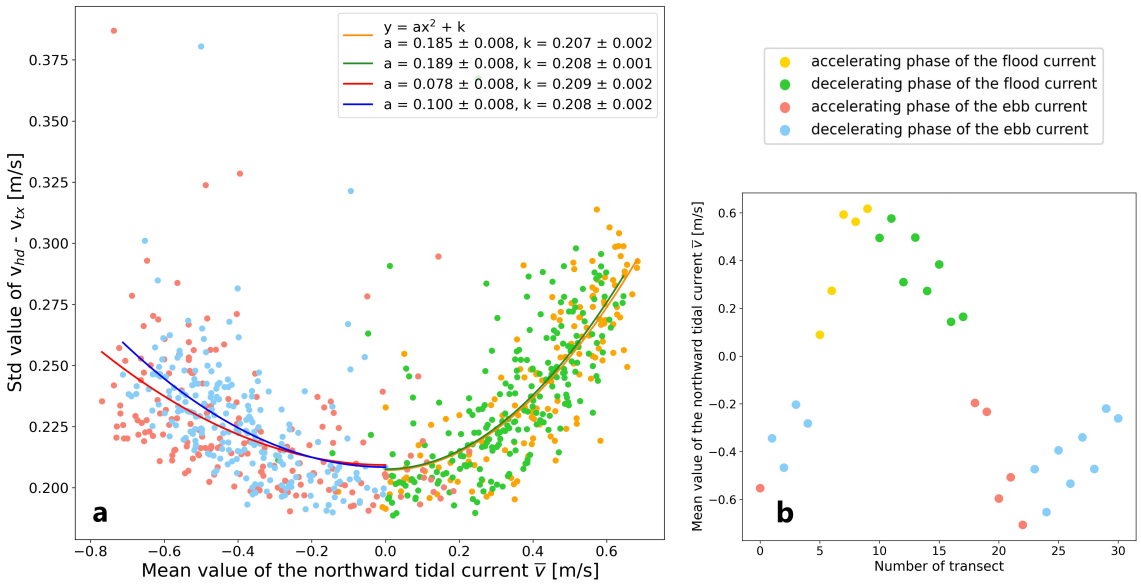

FIGURE 3.6: Subplot (a) corresponds to the standard deviation of the northward velocities' difference between the two ADCPs as a function of the magnitude of the tidal current, which is averaged across the inlet and depths, for the 32 transects of one month (July 2021). Subplot (b) illustrates the four phases of the northward tidal cycle. The four phases are represented by different colors of the scatters. The different colored lines represent the fitted lines between the standard deviation of the difference of the northward velocities and tidal currents for each phase.

tidal flood and ebb currents during the early stage of their decelerating phase of the tidal cycle. Secondly, turbulence decays faster during their decelerating phase and it is generated slowly during their accelerating phase of the tidal currents. This observation indicates a time delay of the turbulence's generation at the seabed. We speculate that during the early stage of the accelerating phase of the tidal current, the turbulence has not been generated yet. At the maximum tidal current velocity, turbulence starts appearing close to the bottom boundary layer. At the late phase of the flood and ebb, when the tidal currents decelerate, turbulence finally becomes manifest at greater heights away from the seabed. Then, the turbulent energy diffuses upwards until the next phase of the tide.

3.2.3.2 Vertical profile of the turbulence

We have concluded that turbulence depends on the strength and the phase of the tide. But how does it vary with depth? Subplots (a) and (b) in Figure 3.7 show the standard deviation of the horizontal eastward and northward velocities' difference respectively as a function of depth. The results are daily averaged. In other words, we compute the standard deviation of the normal distributions of the horizontal water velocities' difference for each depth for each transect in one day and then we take the average of those 32 values. The two different colors represent two different days with different wind conditions and similar current strengths in terms of the variations induced by the spring-neap cycle. The blue points represent the results of July 20, 2021 while the red points represent the results of July 28, 2021. On July 20 (28), 2021, the wind blew northeast (southwest) with a daily mean windspeed 2.6 (8.2) m/s. A speed of 2.6 (8.2) m/s corresponds to 2 (5) Beaufort. The direction and the speed of the wind were measured by the Royal Netherlands Meteorological Institute (KNMI) in De Kooy (notated by a red rhombus in subfigure (b) in Figure 1.1). We observe that the results for the two days follow a similar pattern. At the seabed, the features of turbulence do not exist due to the influence of friction on the tidal currents (Maas and van Haren, 1987). Within the turbulent boundary layer, near the seabed there is a thin layer where shear effects are dominant (Cengel and Cimbala, 2013) and as a result the magnitude of the current velocity must vanish. A little higher than the seabed, but still within the turbulent boundary layer, the turbulent effects start becoming significant but the flow is still dominated by friction effects. This results to an increase of the velocity in the water column near the bottom and therefore to slight turbulence generation. Near the edge of the turbulent boundary layer, the turbulent effects dominate over friction effects (Cengel and Cimbala, 2013), reaching its maximum at around a depth

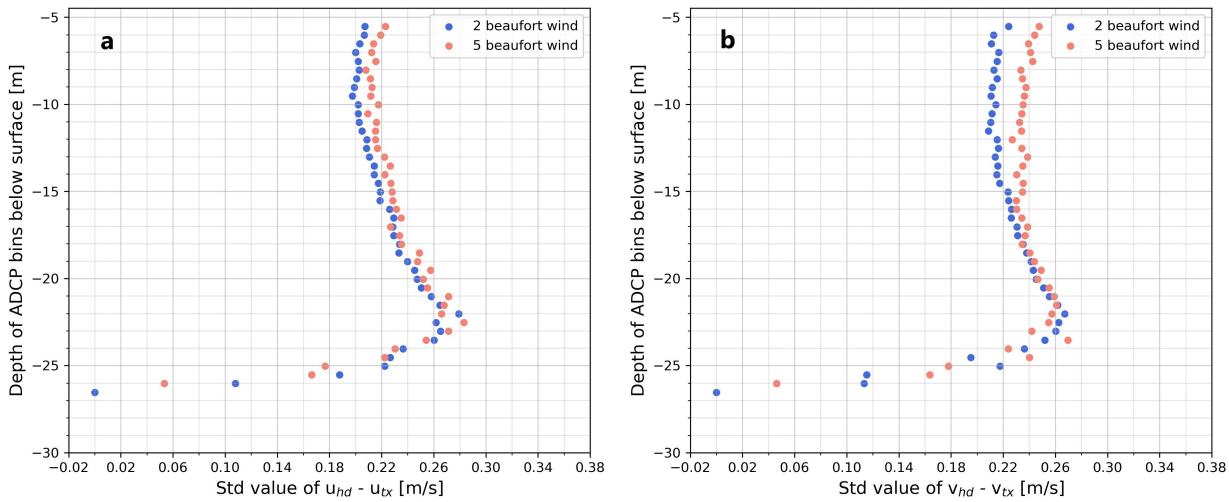

FIGURE 3.7: Standard deviation of the eastward (subplot (a)) and northward (subplot (b)) velocities' difference between the two ADCPs as a function of depth. The results are daily averaged. The two different colors represent two different days with different wind conditions. The blue points represent the results on July 20, 2021 (with daily mean windspeed 2 beaufort) while the red points represent the results on July 28, 2021 (with daily mean windspeed 5 beaufort).

of 22-23m in our case. This explains the fact that we do not observe turbulence exactly at the bottom, because there is continuous conflict with the bottom boundary effect and only slightly above the bottom, it is strong enough to express itself. From that depth upwards, turbulence starts decreasing. At around 8-10m the standard deviation of the horizontal velocity difference is found 0.2 m/s for the calm day and 0.22 m/s for the windy day, both of which correspond to the instrumental noise level that we have already discussed which indicates that at these depth, the environmental turbulence is absent or very small to be measured. As we approach the sea surface, the turbulence slightly increases. We speculate that this increase occurs due to the ferry's motion. While the ferry sails, the flow underneath the hull is disturbed and therefore an additional artificial turbulence takes place.

Moreover, it is worth mentioning that during the windy day, turbulence near the surface is larger than during the calm day. We speculate that this additional turbulence exists due to generation of breaking surface waves. During the windy day, the wind was blowing from southwest to the northeast which means that wind induced waves were propagating from the southern North Sea to the Marsdiep basin and more specifically in the Texelstroom channel. Along this direction, there is no land which could obstruct their propagation and as a result the wind fetch is longer. Therefore, the longer the fetch and the faster the wind, the higher the probability for wave breaking to occur at the sea surface. The presence of those breaking waves enhances the features of turbulence near the sea surface.

Chapter 4

Influence of the ferry's motion on the velocity components in the vertical direction

So far, the ship-induced effect has not been taken into account in the correction of the ADCP data. By using the data as we process it now, it is difficult to extract information regarding the real velocities, especially in the vertical direction, due to the contamination of the data by the ship-induced effect. Our purposes are, firstly, to identify this effect in the vertical direction by analyzing the velocities of the tidal currents and secondly, to correct the data given the existence of the aforementioned effect. In this chapter we present: evidence that the ship-induced effect is present in the ADCPs' measurements and, a first attempt of its elimination.

4.1 Introduction

As we mentioned in Chapter 1, the previous studies in the Marsdiep inlet which used the ADCP measurements mounted on the TESO ferry, were based on the streamwise and the transverse currents and their vertical profiles. The ADCP also measures the vertical velocity of the currents which flow in the Marsdiep inlet. From the vertical velocity measurements we can extract information regarding circulation that may be taking place in the vertical direction or other features that may be present in the Marsdiep inlet such as internal waves or "boils". In this study, for the first time, we look into the profile of the vertical velocity of the currents that flow in the Marsdiep inlet. Figure 4.1 shows the structure of the vertical current speed in the Marsdiep inlet as measured by the two ADCPs during two crossings on July 15, 2021. Subplots (a) and (c) correspond to the 5th crossing of the ferry (between 08:30 and 09:00 CEST) and subplots (b) and (d) correspond to the 28th crossing (between 20:00 and 20:30 CEST). During the 5th transect, the ferry sails from Den Helder to Texel, while at the 28th, the ferry sails from Texel to Den Helder (indicated by a thick arrow at the bottom of the panel). The top panels show measurements by the ADCP that sits on the Den Helder side of the ferry (indicated at the top as *hd*) while the lower panels show that measurements from the Texel side (*tx*). By looking at the two cases, we observe that the two ADCPs measure opposite vertical velocities in one crossing. During the 5th transect, the *hd* ADCP measures positive vertical velocities while the *tx* ADCP measures negative vertical velocities, with 0.25 m/s being the maximum absolute value. The opposite happens during the 28th transect. Consequently, the vertical velocities that the ADCPs measure depend on the sailing direction of the ferry. The ADCP which is located at the rear of the ferry always measures positive vertical velocities whereas, the ADCP which is located in front of the ferry always measures negative vertical velocities. One possible explanation for this observation is that the measurements of the water velocity are affected by the ferry's motion and we strive to take this effect into account in our correction. Specifically, we speculate that as the ferry moves forward the water is pushed down, in front of the ferry, resulting in negative vertical velocities while at the rear of the ferry, the water flows upwards filling the empty space the ship leaves in its passing. A sketch of the ferry and the motion of the flow in its front and rear is illustrated in Figure 4.1. However, there are two similarities between the two ADCPs which are independent of the ferry's direction. The vertical profile of the vertical velocity is uniform along the cross section of the Marsdiep inlet, and it decays with depth.

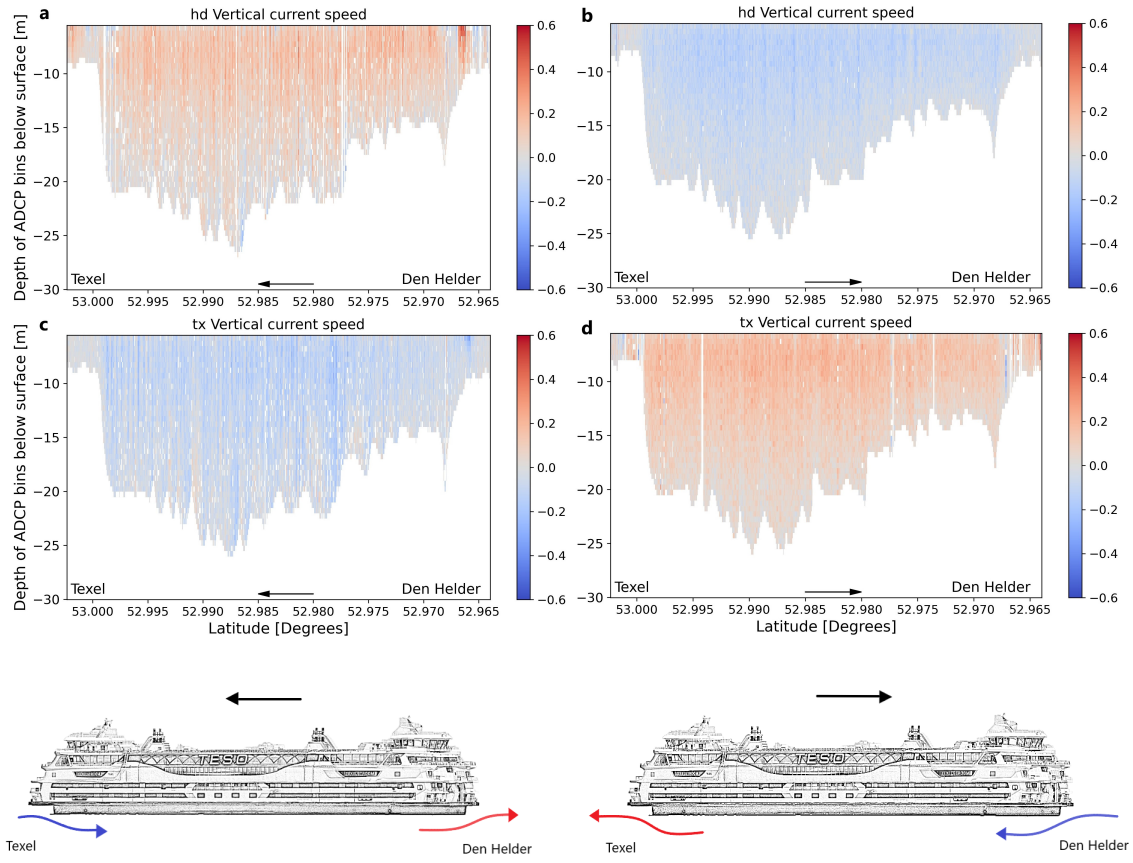

FIGURE 4.1: The vertical profile of the vertical water velocity that the two ADCPs measured across the Marsdiep inlet on July 15, 2021, during the 5th (subplots (a) and (c)) and 28th (subplots (b) and (d)) crossing of the TESO ferry. During the 5th crossing the ferry sails from Den Helder to Texel while during the 28th crossing the ferry sails from Texel to Den Helder as the black arrows notate. Below the subplots, sketches of the ferry's motion for each transect is given (direction indicated by black arrows). The blue arrows correspond to the downward motion of the water in front of the ferry, while the red arrows correspond to the upward motion of the flow at the rear of the ferry.

4.2 Results

4.2.1 Influence of the ferry's motion on the vertical velocity measurements

The vertical profile of the vertical component of the current velocity at latitude 52.9876°N for two transects is illustrated in Figure 4.2 in subplots (a) and (b). It is clear that the vertical velocity of the water measured by the two ADCPs decays with increasing distance from the surface. Subplots (c) through (f) in Figure 4.2 show that the vertical velocity measured by the two ADCPs during the 5th and the 28th crossings of the ferry on July 15, 2021, at that specific location, decays linearly away from the ferry reaching zero at approximately 20-26 m with a decay scale close to 0.07 s^{-1}. Moreover, we observe that the decay scale of the vertical velocity measured by the ADCP which is located at the front (rear) of the ferry is negative (positive) as we expected due to the motion of the water underneath the ferry. We note here that the direction of the ferry's motion determines which ADCP is the front one and which the rear one. For example, during the 5th (28th) transect, the front ADCP is the *tx* (*hd*) and that can be determined by looking at the black arrow in Figure 4.2 which correpsonds to the direction of the ferry's motion.

The decay scale, dw/dz, is computed for each spatial grid in the domain and it is illustrated as a function of latitude in Figure 4.3 for each ADCP separately. The decay scale of the vertical velocity is fairly constant in the middle of the domain (where the ship moves with relatively constant velocity). Near the coasts (where

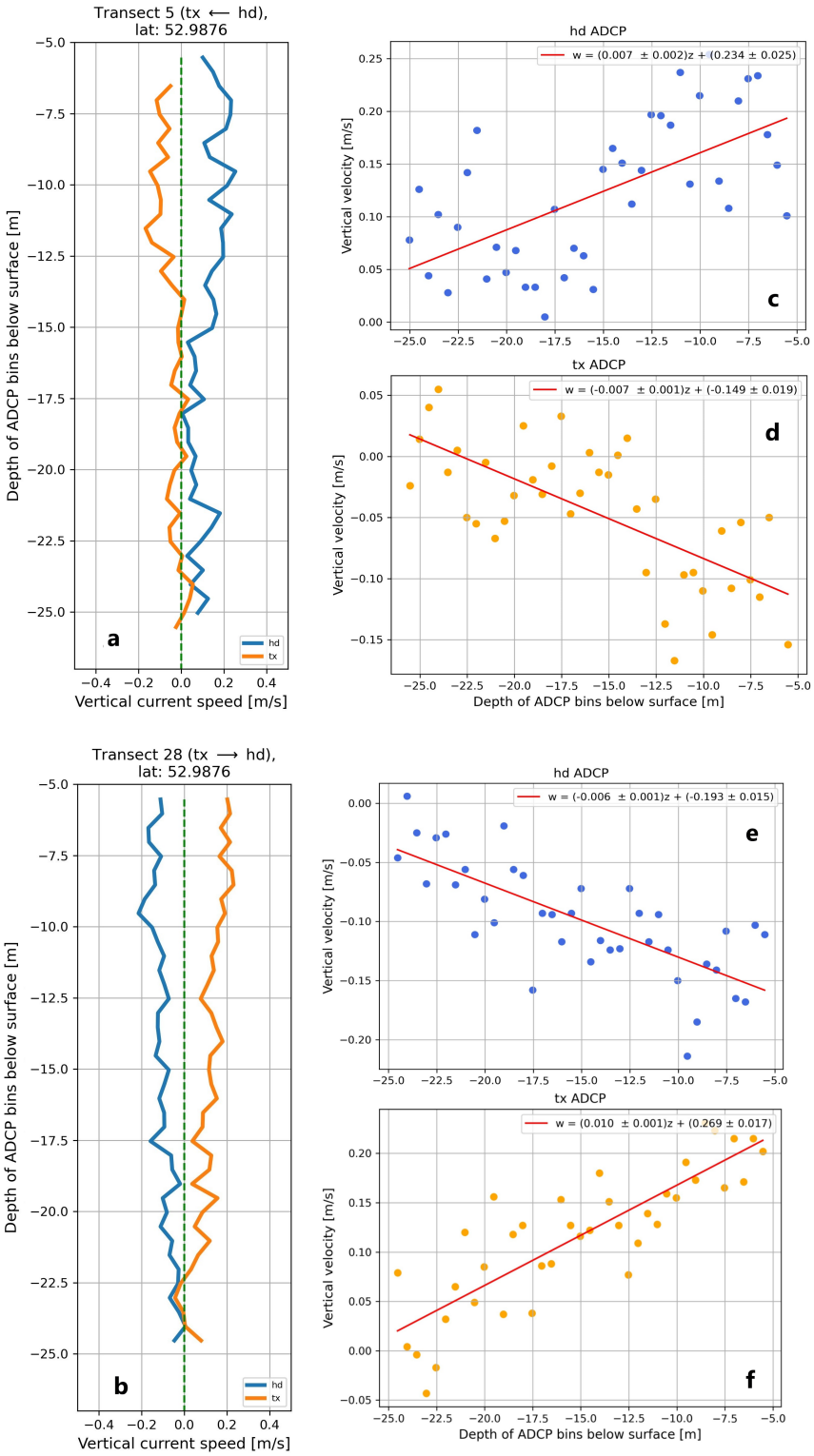

FIGURE 4.2: Subplots (a) and (b) show the vertical profile of the vertical velocity measured by the two ADCPs at the specific latitude 52.9876°N during transects 5 and 28 on July 15, 2021, respectively. Subplots (c) and (d) show the linear relationship between the depth and the vertical velocity measured by the two ADCPs at latitude 52.9876°N during the 5th transect. Subplots (e) and (f) show the results for the 28th transect. The red line corresponds to the fitted line, its slope presents the decay scale of the vertical velocity over the depth and its intercept with y-axis corresponds to the vertical velocity on the sea surface.

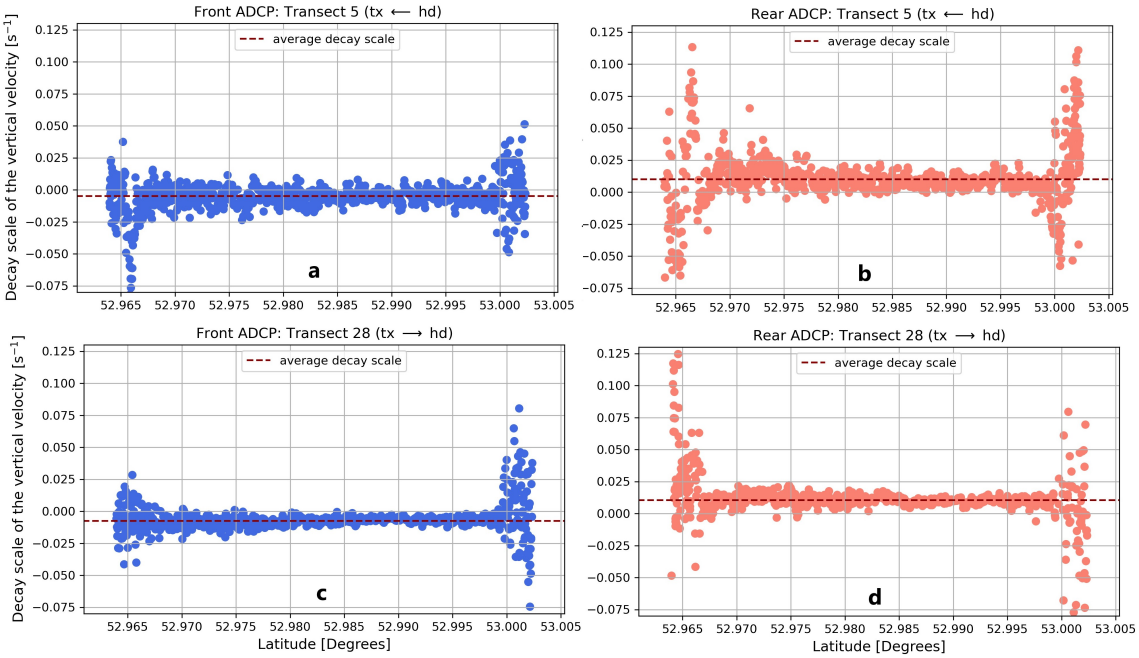

FIGURE 4.3: Decay scale of the vertical velocity as a function of latitude. Subplots (a) and (b) correspond to the 5th crossing whereas subplots (c) and (d) correspond to the 28th crossing of the ferry on July 15, 2021. The results are given for the front and rear ADCP separately. The front and the rear ADCP are determined by the direction of the ferry's motion. During the 5th (28th) transect, the front ADCP is the *tx* (*hd*) ADCP.

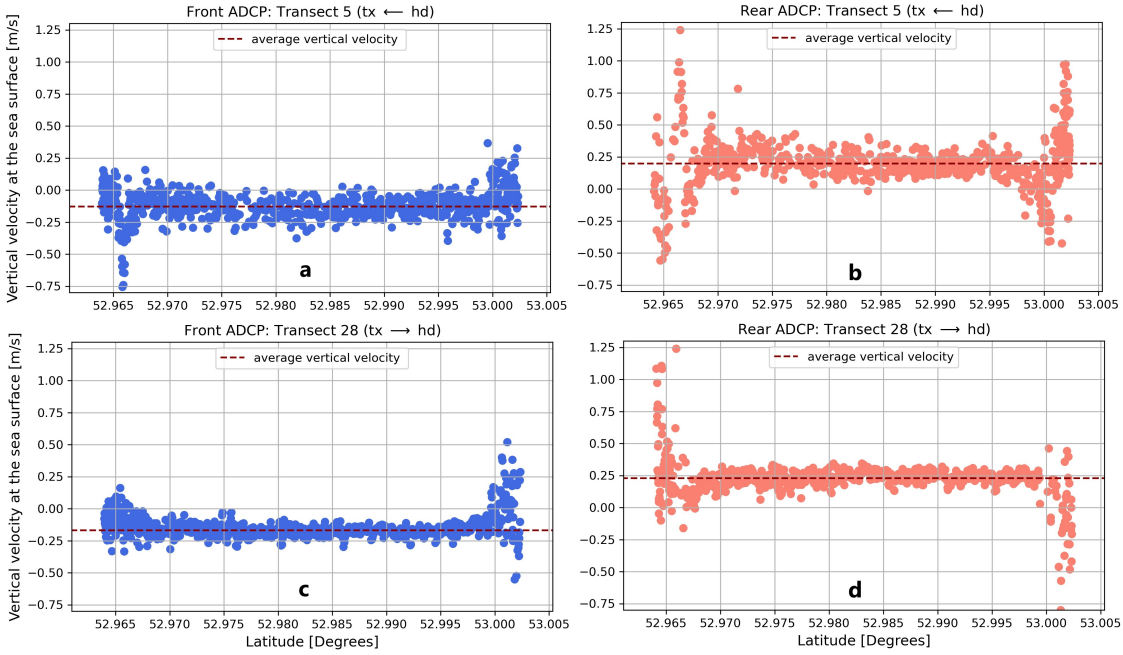

FIGURE 4.4: The vertical velocity on the surface as a function of latitude. Subplots (a) and (b) correspond to the 5th crossing whereas subplots (c) and (d) correspond to the 28th crossing of the ferry on July 15, 2021. The results are given for the front and rear ADCP separately. The front and the rear ADCP are determined by the direction of the ferry's motion. During the 5th (28th) transect, the front ADCP is the *tx* (*hd*) ADCP.

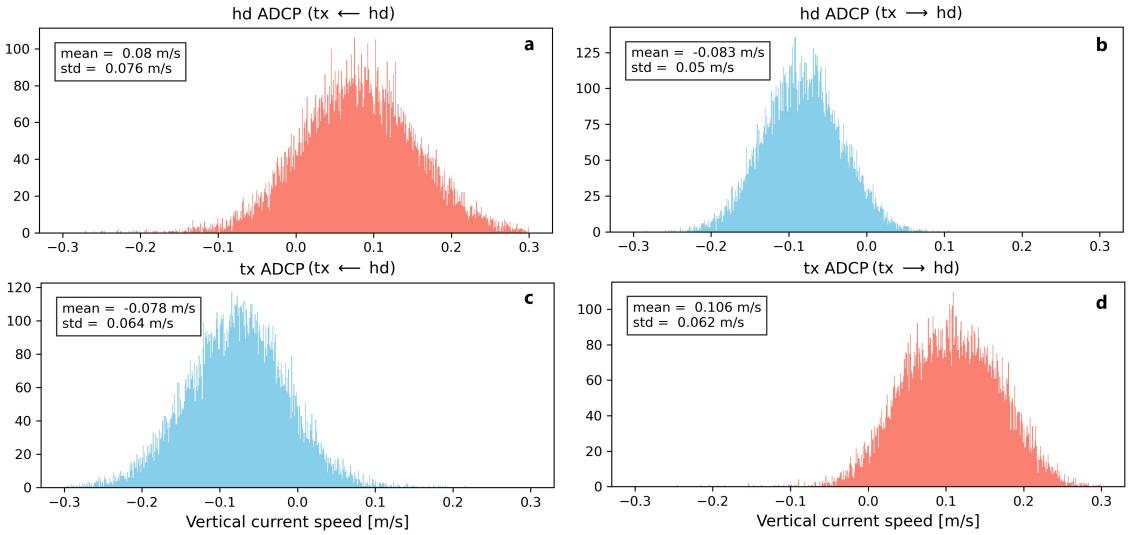

FIGURE 4.5: Normal distributions of the vertical velocities that the two ADCPs measure across the Marsdiep inlet on July 15, 2021, during the 5th (subplots (a) and (c)) and 28th (subplots (b) and (d)) crossings of the TESO ferry. During the 5th crossing the ferry sails from Den Helder to Texel while during the 28th corssing the ferry sails from Texel to Den Helder as the small arrows notate above each subplot.

the ship accelerates and decelerates), the decay scales take larger absolute values, up to 0.125 s^{-1}. If we ignore the measurements near the coasts, then the averaged decay scale of the vertical velocity measured by the front ADCP is found -0.005 s^{-1} and -0.008 s^{-1}, whereas the decay scale of the vertical velocity measured by the rear ADCP is found 0.0100 s^{-1} and 0.0104 s^{-1} during the 5th and 28th transects respectively. Therefore, we conclude that the result differs between a pair of front and rear ADCPs during a crossing, and it also varies for each ADCP (front and rear) during two different crossings. Firstly, we observe that the absolute averaged decay scale of the vertical velocity measured at the rear ADCP, during the two crossings, is slightly larger than that measured by the ADCP in the front and secondly, that the absolute value of the decay scale is found larger for the front and the rear ADCP during the 28th crossing than during the 5th crossing of the ferry.

Moreover, the intercept of the linear fitting in subplots (c) through (f) in Figure 4.2 hypothetically represents the vertical velocity on the sea surface. Likewise, the vertical velocity on the surface, is computed for each spatial grid in the domain, illustrated as a function of latitude in Figure 4.4. This velocity behaves similarly to the decay scale across the transect. Its value is fairly constant in the middle of the domain whereas near the coasts, it takes larger absolute values; up to the unrealistic value of 1.25 m/s. If we ignore the measurements near the coasts again, then the averaged vertical velocity on the sea surface measured by the front ADCP is found -0.134 m/s and -0.169 m/s whereas the vertical velocity measured by the rear ADCP is found 0.200 m/s and 0.227 m/s during the 5th and 28th transects respectively. The rear ADCP always gives larger absolute vertical velocity whereas the result significantly differs between the two transects for both ADCPs. Figure 4.5 shows the vertical velocities distributions for the crossings that are depicted in Figure 4.1 (subplots (a) and (c) correpond to the 5th crossing subplots (b) and (d) correspond to the 28th crossing of the TESO ferry on July 15, 2021). We observe that the mean value of the velocity which is measured by the rear ADCP is always larger than that measured by the front ADCP, a fact which confirms our previous results. The difference in the results between the ADCPs was not investigated during this study. Nevertheless, we speculate this is associated with the fanning out effect (Robijns, 2015). During this effect the flow underneath the hull decreases due to an area of low pressure induced by the rotating propeller. As a result large discharge needs to be diverted to the sides and upwards, towards that area, leading to a record of larger velocities at the stern compared to those at the bow.

We have already concluded that the decay scale of the vertical velocity as well as its value at the surface remain constant in the middle of the transect. However, both variables differ between the 5th and 28th

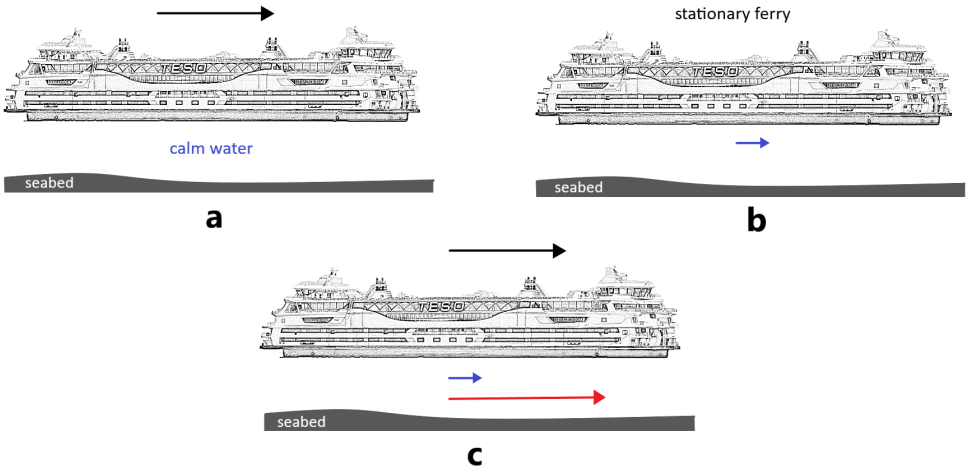

FIGURE 4.6: The sketch illustrates the bottom track velocity divided in two velocity components. The black vector in subfigure (a) is the velocity of the ferry through calm water as measured by the moving ADCP whereas the blue vector in subfigure (b) corresponds to the undisturbed environmental flow as measured by an ADCP stationary with respect to the seabed. In subfigure (c), the red vector corresponds to the sum of the black and blue vectors, which is the velocity of the ferry relative to the seabed (the opposite to bottom track velocity).

transects. By taking into account the ferry's motion influence, we look at the bottom track velocity measurements which correspond to the fictitious velocity of the bottom as measured by the moving ferry. We expect that the ferry's velocity differs from one transect to another. As a result the vertical velocity varies between the two transects. In our analysis we use the velocity of the ferry relative to the water. The bottom track velocity is the sum of the ferry's velocity and the environmental northward velocity which flows along the line of the ferry's motion as shown in the sketch in Figure 4.6. The bottom track velocity is the velocity of the seabed relative to the moving ADCP in a moving medium (flow). The velocity of the ferry relative to the seabed is the exact opposite and it is notated by the red vector in subfigure (c). The black vector is the velocity of the ferry through calm water as measured by the moving ADCP (subfigure (a)) and the blue vector corresponds to the undisturbed environmental flow as measured by a stationary ADCP (subfigure (b)). The red vector is the sum of the blue and black vectors. However, as we previously mentioned, the velocity measurements in the northward direction may be affected by the ship-induced backflow (Chapter 5). Therefore, as shown below, we roughly estimate the environmental northward flow by using the eastward velocity which is hardly affected by the ferry's motion and hence we expect better results.

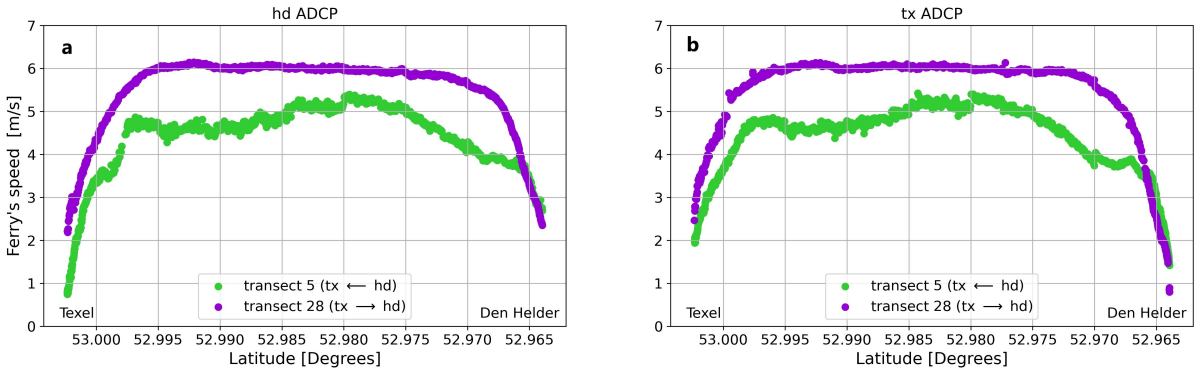

FIGURE 4.7: Ferry's velocity relative to the water as a function of latitude for the 5th and 28th crossings of the ferry on July 15, 2021. The results are given for the *hd* and *tx* ADCP separately. The green points correspond to the 5th transect whereas the violet points correspond to the 28th transect.

The tidal currents do not flow perpendicular to the ferry's trajectory but they flow into/out of the Wadden Sea through Texelstroom (subfigure (a) in Figure 1.1) at an angle. Buijsman, 2007 defined the axis along which the tidal currents flow into and out of the Wadden Sea as the streamwise axis. One convenient resolution of the streamwise current can be achieved by use of the eastward and the northward axes; the velocities along those axes are readily available by the ADCPs. The counterclockwise orientation of the streamwise axis with the eastward-axis is the inclination ψ. The eastward currents and the inclination ψ are known and therefore we can estimate the northward velocity of the flow using the following equation:

$$v_{est} = u_{ADCP} \tan(\psi) \tag{4.1}$$

where u_{ADCP} is the depth-averaged eastward velocity. Note that this method presupposes that the tidal flow is strictly rectilinear, oriented in the ψ direction. In reality, the tidal current profile may be elliptical and as a result the inclination ψ may vary across the inlet. Roughly estimated, the inclination is 10° close to Den Helder, 21° between 52.970°N and 52.980°N, 32° between 52.980°N and 52.995°N and 27° close to Texel (Buijsman, 2007). In this study, we will restrain ourselves and only work with this rough estimation of the northward velocity. Finally this estimation of the northward velocity is subtracted from the bottom track velocity (v_{bt}) to get the ferry's velocity relative to the water (v_f) as follows:

$$v_f = v_{bt} - v_{est} \tag{4.2}$$

Figure 4.7 illustrates the ferry's velocity (v_f) across the 5th and 28th transects on July 15, 2021 for both ADCPs. We observe that the velocity of the ferry, in the middle of the domain, differs between the two transects as we expected. During the 5th transect, the ferry sails with roughly 5 m/s whereas during the 28th transect, it sails with 6 m/s approximately.

Consequently, it is worth searching for a relation between the vertical velocities measured by the two ADCPs and the ferry's velocity. To achieve this, the relationship between the ferry's velocity and the decay scale of the vertical velocity as well as of the vertical velocity on the surface are studied, for the 32 transects of each day over 6 days (from July 12 to July 17, 2021). The ferry's velocity, the decay scale of the vertical velocity as well as the vertical velocity at the surface are averaged across the inlet excluding latitudes close to the harbors. To be more specific, the data which is used for the analysis lies between the 52.967°N and 52.999°N latitude. The results are shown in Figure 4.8 and Figure 4.9 for each variable separately. Subplots

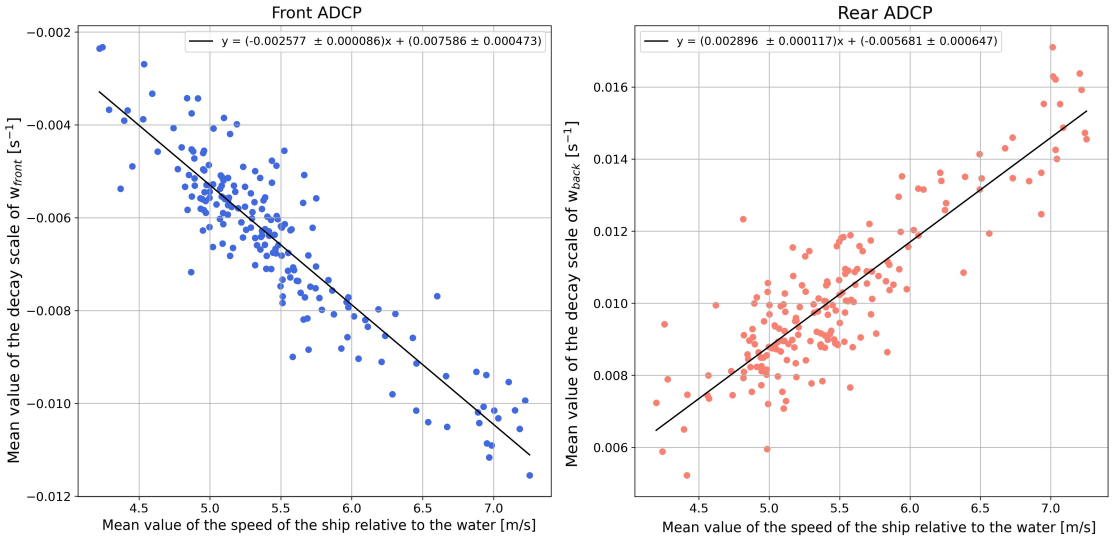

FIGURE 4.8: Decay scale of the vertical velocity as a function of the ferry's velocity, both averaged across the inlet excluding the harbors, for the 32 transects of the day for 6 days (from July 12 to July 17, 2021). The results are given for the front and rear ADCP separately. The black line represents the fitted line, indicating the linear relationship between the two variables.

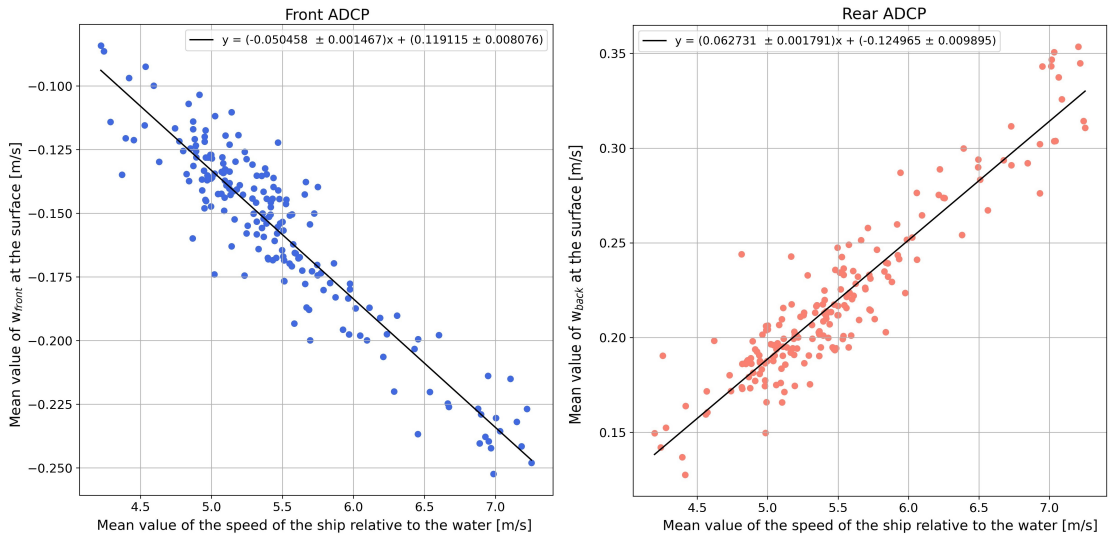

FIGURE 4.9: Vertical velocity computed on the sea surface as a function of the ferry's velocity, both averaged across the inlet excluding the harbors, for the 32 transects of the day for 6 days (from July 12 to July 17, 2021). The results are given for the front and rear ADCP separately. The black line represents the fitted line, indicating the linear relationship between the two variables.

(a) in both figures shows the results for the ADCP located at the front of the ferry while the right subplot shows the result for the ADCP located at the rear of the ferry. We fit the data to find their correlation; we find a linear relationship in both cases. In other words, the absolute decay scale of the vertical velocity as well as of the absolute vertical velocity of the flow at the sea surface increase (decrease) linearly with the increase (decrease) of the ferry's velocity. By combining the two results, we obtain the function below which describes the correction of the vertical velocity profile measured by the ADCPs for the ferry's velocity:

$$w_{fc} = (A\,|v_f| + B)\,z + (C\,|v_f| + D) \tag{4.3}$$

where z is the depth and $|v_f|$ is the absolute ferry's speed relative to the water. The unknown coefficients A, B, C and D can be found via the fitting process, to be discussed below.

4.2.2 Correction of the vertical current speed

As we mentioned in Section 4.1, the ADCP which is located at the rear (front) of the ferry always measures positive (negative) vertical velocities. As a result, the measurements extracted by the rear (front) ADCP show a net upwelling (downwelling) vertical motion of the sea water along the transect. But in reality (in the undisturbed sea), this is not the case. There is no net vertical motion of the water and hence the mean value of the vertical velocity of the flow along the whole transect should be zero. Consequently, as a first correction of the vertical velocity data, we tried to eliminate the net vertical transport of the water, by setting the mean value of the vertical current velocity to zero. To achieve this we firstly compute the horizontally averaged vertical velocity along the inlet (excluding the harbors) for each depth layer ($\overline{w}_{per\,depth}$) namely, the correction term. Then, by subtracting the correction term from the ADCP vertical velocity (w_{ADCP}), we obtain the corrected data for the vertical velocity. This first correction (hereafter "C1"), is summarized in the equation below:

$$(w_{cor})_{C1} = w_{ADCP} - \overline{w}_{per\,depth} \tag{4.4}$$

The following plots serve as an example of the C1 correction scheme, for the 5th crossing of the ferry on July 15, 2021. The profile of the vertical velocity measured by the two ADCPs during this transect is illustrated in Figure 4.1 in subplots (a) and (c). Figure 4.10, presents the results after the implementation of the C1 correction scheme (namely, we make use of eq. (4.4)) in the measurements for each ADCP separately.

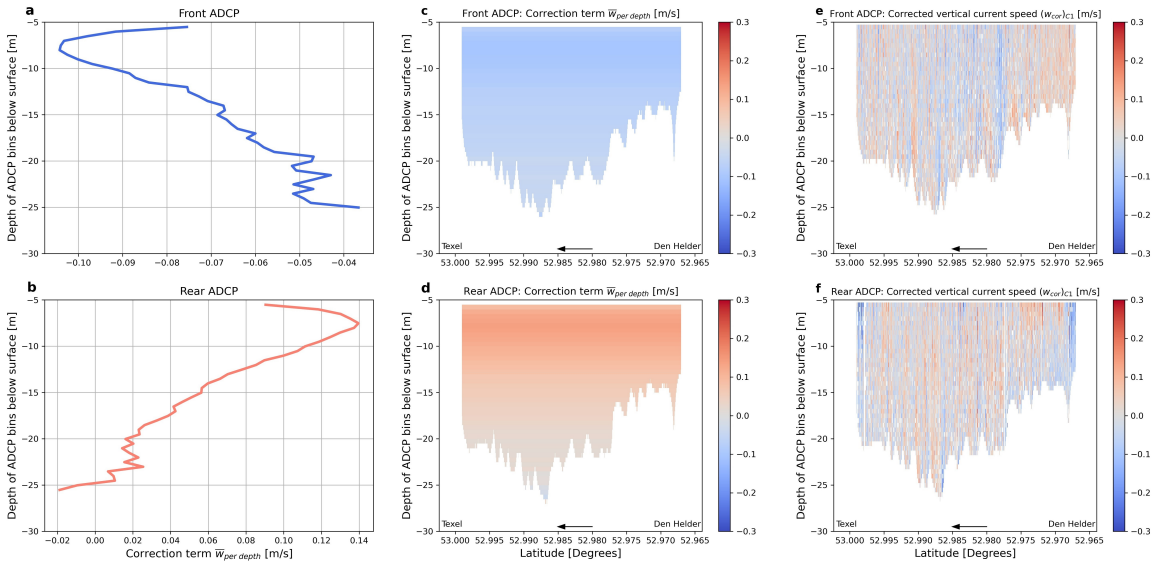

FIGURE 4.10: Implementation of the C1 correction scheme on the vertical velocity during the 5th crossing of the ferry on July 15, 2021. Subplots (a) and (b) present the averaged vertical velocity along the inlet (excluding latitudes close to the harbors) for each depth layer for the front and the rear ADCP respectively. Subplots (c) and (d) depict the correction term of C1 scheme, $\overline{w}_{per\ depth}$, while subplots (e) and (f) depict the corrected vertical velocity $(w_{cor})_{C1}$ for the front and the rear ADCP respectively.

Subplots (a) and (b) present the averaged vertical velocity along the inlet (excluding latitudes close to the harbors) for each depth layer. These are the correction terms to be used for each depth. Subplots (e) and (f) depict the corrected vertical velocity $(w_{cor})_{C1}$ by using the correction terms from subplots (c) and (d). Regarding the correction term, a larger averaged velocity in magnitude is observed between 7-10m of depth for both ADCPs. From that point onwards, the averaged vertical velocity decreases, especially for the rear ADCP which shows a significant velocity reduction over the depth. As for the corrected velocity, although the two ADCPs disagree, there is information that we can extract from their plots by observing some of its features. The results will be discussed in the discussion part.

Although the correction above looks promising, we have not taken into account the ferry's velocity which affects the measurements. Therefore, we keep searching for an additional correction by using the function which describes how the vertical velocity is affected by the ferry's velocity along the depth (eq. (4.3)). First, we fit this function on the data for each ADCP for each transect and we find coefficients A, B, C and D. Then, we substitute in the function, the ferry's speed data computed by eq. (4.2)) as well as the depth measurements and we obtain the estimated vertical velocity (w_{fc}). Then by subtracting the estimated vertical velocity from the ADCP vertical velocity (w_{ADCP}), we obtain the corrected data for the vertical velocity. The correction of the vertical current speed (hereafter "C2") for the ferry speed is summarized in the equation below:

$$(w_{cor})_{C2} = w_{ADCP} - w_{fc} \tag{4.5}$$

where w_{fc} is calculated by eq. (4.3) which takes the following forms for the front and rear ADCP:

$$(w_{fc})_{front} = (-0.00177\,|v_f| + 0.00448)\,z + (-0.05708\,|v_f| + 0.14338)$$

$$(w_{fc})_{rear} = (0.00254\,|v_f| - 0.00375)\,z + (0.06352\,|v_f| - 0.11455)$$

Figure 4.11 presents the results, corrected using the C2 correction scheme, for the same transect as in C1. Subplots (a) and (b) present the correction terms $(w_{fc})_{front}$ and $(w_{fc})_{rear}$ respectively and subplots (c) and (d) show the corrected vertical velocity for the ferry speed, $(w_{cor})_{C2}$. This correction term differs from $\overline{w}_{per\ depth}$. Here, larger velocity magnitudes of the correction term are observed near the first depth layer

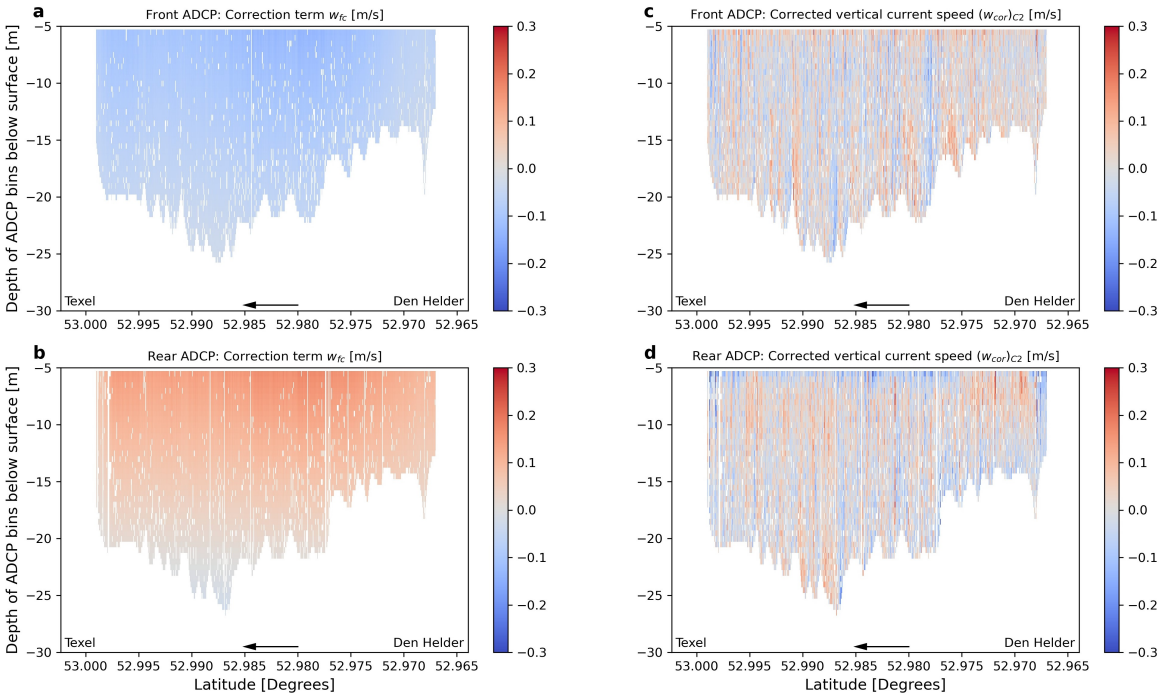

FIGURE 4.11: Implementation of the C2 correction scheme on the vertical velocity during the 5th crossing of the ferry on July 15, 2021. Subplots (a) and (b) illustrate the correction term of C2, w_{fc}, while subplots (c) and (d) depict the corrected vertical velocity $(w_{cor})_{C2}$ for the front and the rear ADCP respectively.

under the ADCPs. Then, it decays as the depth increases, and we observe that the rear ADCP shows a steep velocity decay, just like before. Looking at the corrected velocity, although the two ADCPs disagree, we observe that they each follow a similar pattern to their counterpart in the C1 scheme. The results of C1 and C2 share some common features which will be discussed later but there are some notable differences as well. The most important of the differences here is that at the first depth layer below the ADCPs, there is a dark red (blue) band for the front (rear) ADCP which suggests that there is upwelling (downwelling) motion of the flow at the sea surface. We are not sure if this is physically feasible. One speculation is that this upwelling (downwelling) motion of the flow at the sea surface are caused by lateral flow components which flow to and from the sides of the ferry, induced by the ferry's motion. Nevertheless, it seems that although we applied the correction for the ferry's speed, the ferry's effect on the vertical velocity has not been fully eliminated.

Therefore, in our last attempt to eliminate this effect, we came with a third correction scheme (hereafter "C3"). Instead of applying the function of the ferry's velocity directly on the measured data, as done by C2, we apply it to the corrected vertical current velocities from C1. In other words, we combine C1 and C2. To do that, we must first fit the ferry's speed function, not on the ADCP data but rather on the ADCP corrected (by C1) data, to find coefficients A, B, C and D. We use this fit to calculate the estimated vertical velocity correction. We then subtract the correction term from the corrected (by C1) vertical velocities:

$$(w_{cor})_{C3} = (w_{cor})_{C1} - w_{fc} \tag{4.6}$$

where w_{fc} is calculated by eq. (4.3) which takes the following forms for the front and rear ADCP as follows:

$$(w_{fc})_{front} = (-0.00165\,|v_f| + 0.00734)\,z + (-0.05622\,|v_f| + 0.26090)$$

$$(w_{fc})_{rear} = (0.00246\,|v_f| - 0.01142)\,z + (0.06364\,|v_f| - 0.29760)$$

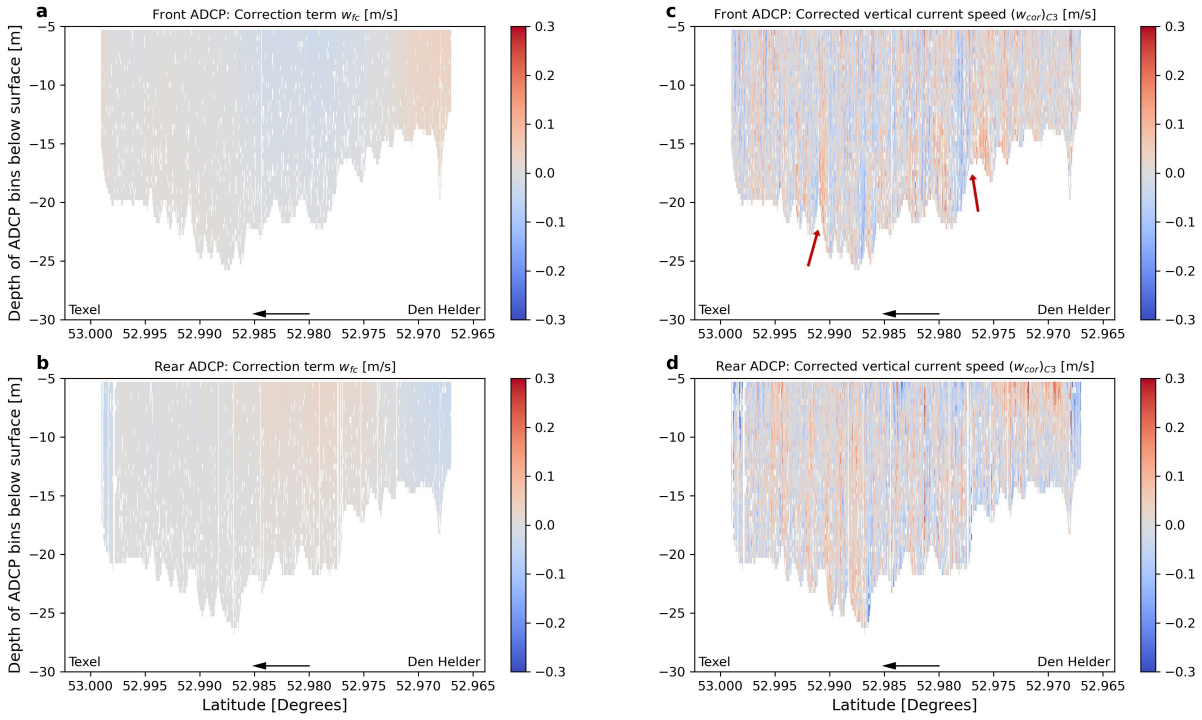

FIGURE 4.12: Implementation of the C3 correction scheme on the vertical velocity during the 5th crossing of the ferry on July 15, 2021. Subplots (a) and (b) illustrate the correction term of C3, w_{fc}, while subplots (c) and (d) depict the corrected vertical velocity $(w_{cor})_{C3}$ for the front and the rear ADCP respectively. The two small red arrows in subplot (c) show the strongest downwelling and upwelling motion of the flow that were observed at the steepest slopes of the topography.

Figure 4.12 presents the results of the C3 correction scheme. Subplots (a) and (b) present the correction terms $(w_{fc})_{front}$ and $(w_{fc})_{rear}$ respectively and subplots (c) and (d) give the corrected (by C3) vertical velocity, $(w_{cor})_{C3}$. The correction term in subplots (a) and (b) does not vary vertically, in contrast to the previous two schemes where the correction term decayed with increasing depth. Additionally, C3's correction term also differs horizontally from C1's and C2's because the correction term varies along the transect. This variation reflects the variation of the ferry's speed along the transect as illustrated with green in Figure 4.7. Near the harbor of Den Helder, between 52.967°N and 52.970°N latitude, a significant speed reduction is observed. This reduction may be associated with the red (blue) color that is observed in subplots (a) and (b) in Figure 4.12 for the front (rear) ADCP at that location. Moreover, the corrected velocity of the C3 scheme follows a similar pattern to the other two schemes' corrected velocities. However, there are a few noteworthy differences among these three corrections that we will investigate in Section 4.3.1.

4.3 Discussion

4.3.1 The best vertical velocity correction yet

Section 4.2.2 presents the results of the three correction schemes that we proposed for the vertical current velocity, along with a brief report on the similarities and differences among them. The differences among the three corrections are observed either near the surface, at the first depth layer below the ADCP or close to the harbors. C2 and C3 give smaller vertical velocity magnitudes for the front ADCP close to Den Helder's harbor compared to C1. This is because in the C1 scheme, we haven't taken into account the ferry's speed which affects the measurements. In addition to that, we observe in Figure 4.7, that near the harbor, the speed of the ferry significantly decreases compared to its speed in the middle of the transect. This reduction

may have a notable impact on the vertical velocity, which C2 and C3 managed to capture and deal with. A noteworthy feature is the horizontal band of a dark blue (red) color which exists at the first two depth layers right below the front (rear) ADCP at around 5m as illustrated in Figure 4.11 indicating an apparent strong downwelling (upwelling) motion of the water. This feature is observed only in the C2 scheme, and may be associated with the ship-induced effect. It most probably is an imprint left from the function of the ferry's speed. However, this feature is eliminated in the C3 correction scheme.

It is noteworthy to mention that possible errors in the C2 and C3 schemes may originate from an erroneous interpretation of the decay of the vertical velocity. In section 4.2.1, Figure 4.2 we found a linear decay of the vertical velocity with depth and based on that we corrected the measured vertical velocity through eq. (4.3). This linear dependence on depth is based on a shallow-water response. In this case the presence of shallow-water response is motivated by the fact that the ferry induces a free surface gradient by the displacement of water during its passing (piling up water in front of the ferry and reducing the water level behind it). The pressure gradient acts over the length of the ferry, creating vertically uniform horizontal velocities (over the water column but not near the seabed due to the presence of friction effects). According to the continuity equation dw/dz must be z-independent which implies that w is linear in z (Cushman-Roisin and Beckers, 2011). However in subplots (a) and (b) in Figure 4.10 we observe that the maximum of the vertical velocity lies at a depth of 7-8m instead of at the surface, as the shallow water theory predicts. There may be a potential flow near the ship which may exhibit some kind x,y and z dependence which we do not consider and as a result our approach may not be entirely correct. It seems that eq. (4.2) works well for most depths but it is still incorrect for depths near the surface and therefore an additional term should be included in this equation (quadratic or cubic term). The lack of this term, clearly gives errors in the vertical velocity corrected by the C2 and C3 schemes at these depths.

Furthermore, the most important issue shared by all three correction schemes, is that the results between the two ADCPs always differ significantly. In schemes C2 and C3, we tried to correct for the upwelling/downwelling, but there's still some residual difference between the two ADCPs. Unfortunately, we have not interpreted this residual difference yet. However, by comparing the result of the front and the rear ADCP in subplots (c) and (d) in Figure 4.12 one could say that the result of the front ADCP looks more reliable than the rear one. The features which allow us to believe that, are the dark blue vertical zone between 52.975°N and 52.580°N latitude and the dark red vertical zone close to 52.990°N latitude indicated by the red arrows in Figure 4.12. Thus, we have strong downwelling and upwelling motion of the water in these two locations, that cannot be seen by the rear ADCP due to effects that we may not know of. We speculate, that these two features are associated with the topography of the bottom. This may be a consequence of the flow following the topography. In Figure 4.13 we see that during this transect, the tidal current flows northward. Hence, as the water flows from Den Helder to Texel, when the depth increases (decreases), then the tidal flow goes downwards (upwards) and this explains the blue (red) colors in the two locations. Also, we observe that, the slopes of the topography are the steepest where the strongest upwelling and downwelling motion of the flow occurs.

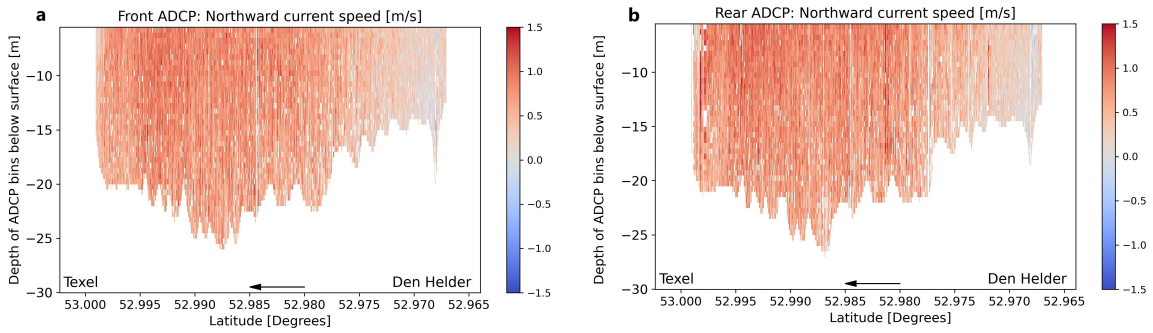

FIGURE 4.13: Northward current velocity measured by the front (subplot (a)) and rear (subplot (b)) ADCP on July 15, 2021 during the 5th crossing of the ferry.

Consequently, the best correction scheme seems to be C3, where the measured vertical velocity by the ADCPs is firstly corrected for the net vertical motion of the flow and then for the ferry's motion. Nevertheless, this correction cannot be considered ideal. Although we managed to identify the topography-induced vertical velocity, evidence for the presence of estuarine circulation, is not visible, as we expected in the C3 scheme. The estuarine circulation is driven by baroclinic (density) pressure gradients which appear due to the motion of the bottom saline inflow water and the surface fresh outflow water in an estuary. According to Ralston and Stacey, 2005; Lerczak and Geyer, 2004, the tidal currents along the channel are strongest in the middle and at the deepest location of the channel and weaker at the shoals. Because of this lateral shear, the along-channel tidal currents are advected with a different speed at different lateral locations. This results in a cross-channel (lateral) density gradient which creates a lateral circulation pattern. For example, during floods, the water in the middle of the channel has higher salinity (higher density) than at the shoals (lower density). Due to this density gradient in the cross-channel direction, saline water flows out onto the shoals near the seabed and shoal water converges at the sea surface. The opposite happens during ebb currents. These features of the estuarine circulation can be seen in the correction term of the C3 scheme in Figure 4.12 in subplot (a). We observe that there is an upwelling motion of the flow near the right edge of the transect and a downwelling motion of the water in the middle of the transect suggesting the presence of a vertical circulation like in the flood case that we have just described. However, as we mentioned in Section 4.2.2 these features may be associated with the ferry's velocity and as a result they are removed in the final correction in our attempt to eliminate the ferry's effect that seems to still exist near the sea surface. Therefore, this correction seems to be working well enough locally in the presence of local phenomena but fails in the presence of large scale phenomena like estuarine circulations.

4.3.2 Search for topography-induced vertical velocity

In the previous section, we found that the strongest upwelling and downwelling motion of the flow occurs on the steepest slopes of the topography by only looking at the measurements of the front ADCP. Empirically, the vertical velocity induced by the topography can be estimated by the following relation:

$$w = -u\,\frac{dh}{dx} - v\,\frac{dh}{dy} \tag{4.7}$$

where w is the vertical velocity (m/s), u is the eastward velocity (m/s), v is the northward velocity (m/s) and dh/dx and dh/dy are the rates of change of depth of the topography (m) with respect to the eastward and northward directions (m), respectively. Note here that the distance of 1° latitude corresponds to 111 km.

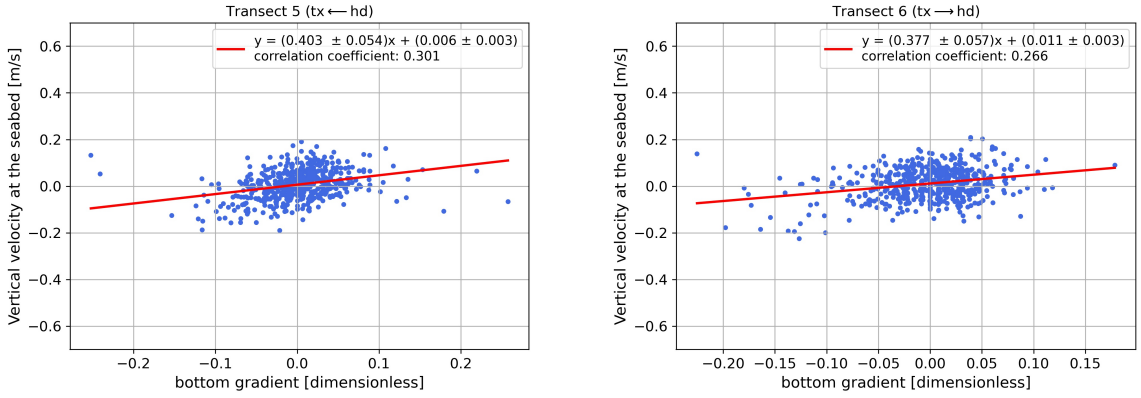

FIGURE 4.14: The vertical velocity near the seabed computed by using the C3 scheme as a function of the bottom gradient for two subsequent transects (5th and 6th transects) on July 15, 2021. The bottom gradient was computed by using two subsequent spatial grids each time. The red straight fitted line corresponds to the northward horizontal velocity of the flow (eq. (4.7)).

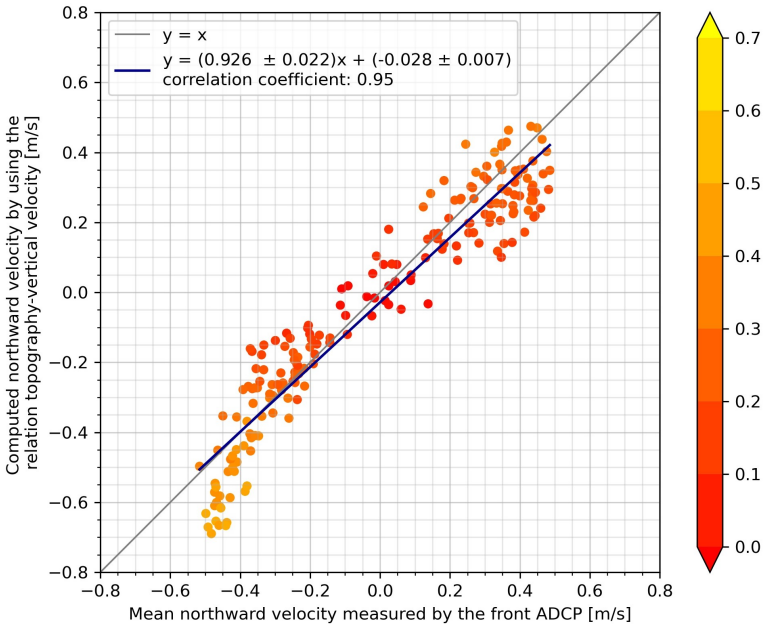

FIGURE 4.15: The relationship between the estimated northward velocity, the value of which is obtained through the slopes of the fitted line of Figure 4.14 (based on the measured vertical velocity and bottom slope, $-\frac{w}{dh/dy}$), and the observed northward velocity which is the northward velocity measured by the ADCP located at the front of the ferry using data for the 32 transects of the day for 6 days (from July 12 to July 17, 2021). The observed northward velocity is averaged along the transect and over 2m above the bed. The straight dark blue line corresponds to the fitted line while the straight grey line represents the line $y = x$. The color of each point represents the correlation coefficient between the bottom gradient and the corrected vertical velocity for each transect (as shown in the legend in Figure 4.14).

By taking the above relation into account, we expect a high correlation and a linear relation between the slope of the bottom in the northward direction and the vertical velocity. Figure 4.14 shows the vertical velocity computed by using the C3 scheme, exactly at the seabed, as a function of the slope of the bottom for two subsequent transects (5th and 6th transects) on July 15, 2021. The slope of the topography was computed by using two subsequent spatial grids each time. As we observe, the linear relationship between the variables is not clearly visible as we expected for both crossings of the ferry. There are scatters and the correlation between them is small ranging from 0.26 and 0.3. However, we follow the fitting process and according to eq. (4.7), the slope of the red fitted line corresponds to the mean northward velocity of the flow near the seabed while the intercept on the y-axis and the scatters correspond to the first term, which involves the eastward velocity and the topography variation in this direction. The relation between the estimated northward velocity through the slopes of Figure 4.14 and the expected northward velocity which is the northward velocity measured by the front ADCP, is presented in Figure 4.15. Note that the latter horizontal velocity is averaged along the transect and over 2m above the bed. Figure 4.15 shows the results for the 32 transects of the day for 6 days (from July 12 to July 17, 2021). The correlation coefficient between the two variables is high; at around 0.95. Also, we observe that the slope of the dark blue fitted line of this figure is found 0.926 which means that the northward velocity estimated by using eq. (4.7) is slightly smaller than the measured northward velocity. Also, in this figure, the colors of each point represent the correlation coefficient between the bottom gradient and the corrected vertical velocity for each transect. We see that its value varies depending on the tidal current. For strong ebb and flood currents, the correlation is between 0.5 and 0.7 whereas for slack tides the correlation is below 0.4. By excluding the odd numbered transects in the calculations (Figure 4.16), i.e the crossings from Den Helder to Texel, we get a higher correlation at around 0.975 while the slope of the dark blue fitted line of this figure is 1.11 which means that the northward velocity estimated by using eq. (4.7) is slightly larger than the measured northward velocity. This indicates

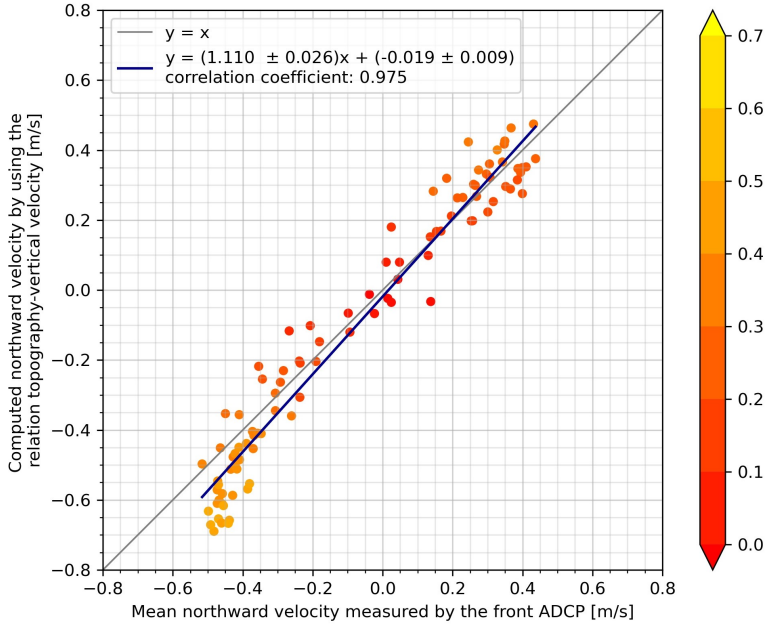

FIGURE 4.16: The relationship between the estimated northward velocity, the value of which is obtained through the slopes of the fitted line of Figure 4.14 (based on the measured vertical velocity and bottom slope, $-\frac{w}{dh/dy}$), and the observed northward velocity which is the northward velocity measured by the ADCP located at the front of the ferry using data for the even numbered transects of the day for 6 days (from July 12 to July 17, 2021). The observed northward velocity is averaged along the transect and over 2m above the bed. The straight dark blue line corresponds to the fitted line while the straight grey line represents the line $y = x$. The color of each point represents the correlation coefficient between the bottom gradient and the corrected vertical velocity for each transect (as shown in the legend in Figure 4.14).

that the first term in eq. (4.7) takes larger values during the crossing from Den Helder to Texel and as a result we can conclude that the bathymetry variations in the eastward direction are larger.

Therefore, we can conclude that eq. (4.7) seems to work well and the strong upwelling and downwelling motion of the flow on the steepest slopes of the topography which are observed in Figure 4.12 correspond to the topography-induced vertical velocity. Nevertheless, we have to keep in mind that the correlation between the slope of the topography and the vertical velocity is still small even if there is almost a 1-1 relation between the northward velocity estimated by using eq. (4.7) and the measured northward velocity. Here, it is important to stress that the topography in the Marsdiep inlet varies not only in the north-south direction but in the east-west direction as well. Even though we have not analysed the bathymetry along the channel in this study, we have to keep in mind that these vertical velocities may also be affected by the flow component perpendicular to the transect and the bottom slope in this direction (first term in eq. (4.7)). Additionally, in Chapter 3, we saw that the magnitude of the eastward velocity is larger than the northward velocity in the tidal cycle and more specifically the former can be two times larger than the latter. Consequently, the contribution of this term significantly influences our results. Note that the bathymetry of the Marsdiep channel can be constructed from the ADCP data and therefore this can be investigated further in future studies. One can say that the result could also be affected by the presence of tide-induced vertical velocity. If we assume that the water level changes by 150 cm between the low and high tide with time difference of 6.125 hours then the tidally induced vertical velocity is estimated at around 0.006 cm/s. Therefore, the magnitude of the vertical velocity induced by tides is much smaller than the vertical velocity induced by topography and thus cannot heavily affect the results.

4.3.3 Physical indications of the corrected vertical velocity plot features

After correcting the vertical velocity, our purpose is to search for physical indications that can be observed visually during a crossing of the TESO ferry. Figure 4.17 shows instances of fronts and a "boil" that were observed in the Marsdiep inlet from the ferry on June 1, 2022 at 15:37 CEST (during the 19th crossing of the ferry). Fronts are visible as foam lines on the water surface and through changes in colors at the sea surface. The fronts are generated due to the converging of different water masses on the surface. In the Marsdiep, the fresher water discharged from Lake IJssel and flowing out of the Wadden Sea through the Malzwin channel combines with the saltier water coming from the North Sea and flowing into the Wadden Sea through the Texelstroom (this happens during the late stage of the ebb tide). These fronts gradually progress northward (Groeskamp, 2008; Buijsman, 2007). Moreover, "boils" are common phenomena in the southern North Sea (Thorpe et al., 2008). They are detectable on the sea surface and they have mean horizontal dimensions of about 25 m. A "boil" is defined as small-scale turbulent upward motion of the flow. It starts from the turbulent boundary layer close to the seabed and it moves upwards until the sea surface. The "boils" are visible as a near-circular region of convergence on the water surface (Thorpe et al., 2008). In Figure 4.17, the "boil" is observed as a brown patch due to the upward motion of enhanced sediment concentration from the seabed to the water column. The "boil" was observed close to the Den Helder harbor, at around 52.977°N.

Figure 4.18 presents the corrected vertical velocity by using the C3 correction scheme, and the echo intensity corrected for transmission losses due to geometrical spreading and fluid attenuation as described in Section 2.3, for that specific transect. Regarding the echo intensity plot, the colors represent the strength of the returned acoustic energy. The higher values indicate more suspended matter in the water. We only focus on the results of the front ADCP (subplot (a) and (b) in Figure 4.18) and we see that, at around 52.977°N, there is a dark red column which corresponds to a strong upwelling motion of the water whereas, at around 52.988°N, there is a dark blue column which corresponds to a strong downwelling motion. By looking at subplot (b) we see that this upwelling motion is associated with high sediment concentration (narrow red column which is notated by red arrow) whereas the downwelling motion is associated with low sediment concentration (narrow light blue column which is notated by blue arrow) in the whole water column. Part of the front lines were perpendicular to the ferry's trajectory at these two locations and therefore the aforementioned features indicate the presence of the front lines as the ferry was crossing through them during its trip. Furthermore, this strong upwelling motion of the flow with enhanced sediment concentration at around

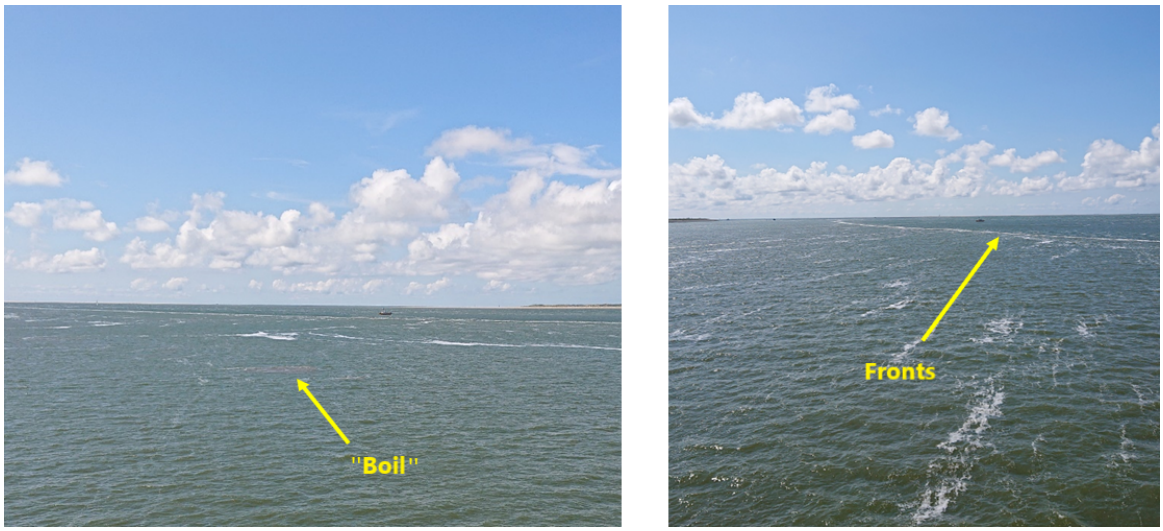

FIGURE 4.17: Features of a "boil" (subfigure (a)) and a front (subfigure (b)). The foam line marks a front and the browinsh circular region marks a "boil" in the Marsdiep inlet. The left photograph was taken by Leo Maas on the TESO ferry on June 1, 2022 at 15:37 CEST and the right photograph was taken a few minutes later (during the 19th crossing of the ferry).

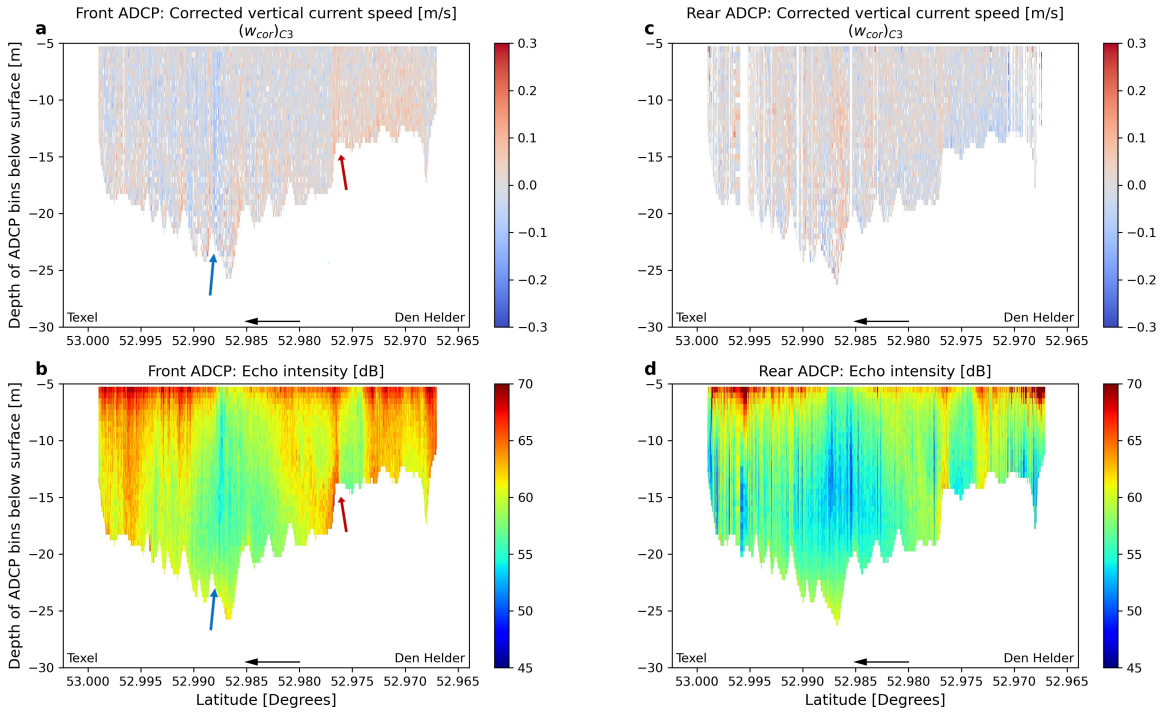

FIGURE 4.18: Subplots (a) and (c) illustrate the corrected vertical velocity computed by using the C3 correction scheme while subplots (b) and (d) show the measured echo intensity which is corrected for transmission losses due to geometrical spreading and fluid attenuation, for the front and the rear ADPC respectively. The plots correspond to the 19th crossing of the ferry on June 1, 2022. The red and blue arrows show the strongest upwelling and downwelling motion of the flow which are associated with high and low sediment concentration in the whole water column and may indicate the presence of physical features there.

52.977°N which covers an area of 20m diameter gives evidence suggesting that a "boil" was present (not the particular one in the photo because that one was not crossed by the ferry). It is noteworthy that this is further evidence that the corrected vertical velocities from the front ADCP are more reliable than those from the rear ADCP because the latter one does not give any evidence for any physical feature at the locations where the fronts and the "boil" take place.

Chapter 5

Influence of the ferry's motion on the velocity components in the sailing direction

The ship-induced effect, which is described in Chapter 4, is not limited to the vertical direction; it affects the horizontal velocity components as well. The ferry travels mainly in the north-south direction between the mainland of the Netherlands (Den Helder) and Texel. As the ferry moves, it displaces a large amount of water from the bow back to the stern of the ferry through a backflow due to a pressure gradient which is created by water level differences. Due to the pressure gradient, the water flows backwards filling the empty space the ferry leaves in its passing. This backflow underneath the hull cannot be eliminated by the ADCPs and as a result it is misinterpreted as a current originating from the tides. Therefore, the measurements of the flow's velocities along the ferry's motion (in the northward direction in this case) are contaminated by this induced backflow. In this chapter, we will try to identify the induced backflow by looking at the ADCP measurements and we will also try to correct them.

5.1 Introduction

In the previous chapter, we looked at the vertical velocity and how it is affected by the ferry's motion. In this section, we investigate the ferry's impact on the along-ferry horizontal velocity component and we attempt to correct it as well. The ship-induced backflow cannot be identified by looking at the velocity profile of each ferry crossing individually. The influence of the ferry's motion on the velocity measurements can be identified by looking at the timeseries of the tidal currents during a day. Figure 5.1 shows the eastward (subplots (a) and (b)) and northward (subplots (c) and (d)) tidal current, measured by the two ADCPs, averaged across the inlet and depth, as a function of the 32 crossings of the ferry on July 12, 2021. The colored points in the subplots indicate the direction of the ferry's motion during each crossing. We observe that both eastward and northward timeseries of the tidal currents measured by the two ADCPs have a sinusoidal behaviour, as expected. However, by comparing the curves of the eastward and northward tidal current, we see that the former is smoother whereas the latter shows zig-zag patterns close to the flood and the ebb currents. We speculate that the presence of this zig-zag pattern is caused by the ship-induced effect which affects the measurements of the currents' velocities. In other words, it seems that the ADCPs might overestimate or underestimate this horizontal velocity component of the flow depending on the direction of the ferry's motion.

We first approach this by estimating this ship-induced backflow, by using the vertical profiles of the northward current velocity measured by the two ADCPs during two subsequent transects. Figure 5.2 illustrates this general approach for the backflow's estimation. The sketch shows two cases in which the ferry sails in opposite directions, at its top indicated by a black arrow. We assume that these two cases correspond to two subsequent crossings of the ferry. Below the ferry, there are three arrows; the orange arrow represents the environmental background flow which includes the tides and the wind-induced flow. The green arrow represents the ship-induced backflow and the purple arrow is the sum of the environmental and the ship-induced flow and it corresponds to the northward velocity measured by the ADCPs. It is important to

stress here that this sketch shows the ideal case: the two orange arrows have the same magnitude and direction which means that the environmental/ tidal flow does not change between these two transects. Also, the green arrows have the same magnitudes and the opposite directions which means that the ferry sails with the same speed through the water during these crossings. Then by taking these two subsequent transects and subtracting the vertical profiles of the horizontal along-track velocities, we should theoretically obtain two times the ship-induced flow as a result. However, the tidal current significantly varies among the ferry crossings and we need to find two subsequent transects in which the environmental flow only changes slightly to minimize the error. Therefore, these two crossings are chosen close to either the maximum flood or ebb when the tidal currents are mostly similar. Lastly, the ferry doesn't actually sail with the same speed each time, a fact that contributes in the error of our assumption, since we theoretically take the speed to be approximately constant. Another possible approach for the estimation of the ship-induced backflow would be to compute the profile of the environmental northward flow through the measured profile of the eastward velocity analysed in Chapter 4 using eqs. (4.1) and (4.2) for each transect. Then by comparing the latter with the measured profile of the northward flow which is acknowledged to be potentially erroneous due to a ship-induced component, we can get the ship-induced backflow.

As the colored arrows indicate in the sketch, we would expect that when the ferry sails from Den Helder to Texel (from Texel to Den Helder) and there is a flood (ebb) current that has a substantial northward component, the ADCPs' measured northward currents should have had smaller magnitudes than the real currents that flows in the inlet. When the ferry sails along the direction of the tidal current, the ship-induced backflow, which always points in the opposite direction of the ferry's motion, weakens the tidal current.

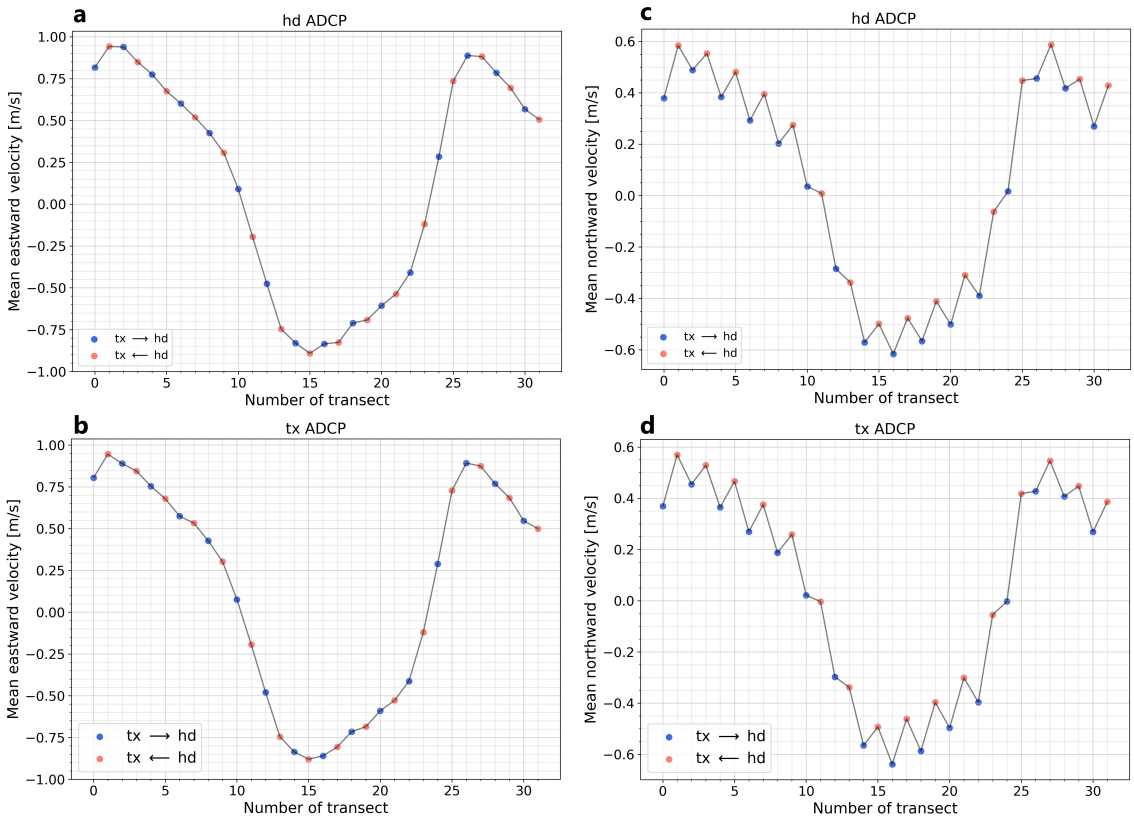

FIGURE 5.1: The eastward (subplots (a) and (b)) and northward (subplots (c) and (d)) tidal current measured by the *hd* and *tx* ADCP, which is averaged across the inlet and depths as a function of the 32 crossings of the ferry on July 12, 2021. The first crossing of the ferry corresponds to the zeroth transect and the 32th crossing correspond to the 31th transect. The blue points denote that during those transects, the ferry sails from Texel to Den Helder whereas the orange points denote that the ferry sails from Den Helder to Texel.

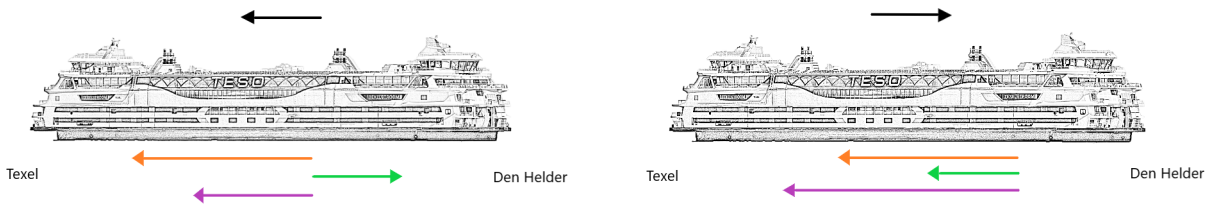

FIGURE 5.2: This sketch illustrates our approach for the computation of the ship-induced backflow. These are two subsequent crossings of the ferry in the Marsdiep inlet. The black arrows show the direction of the ferry's motion. We assume that the velocity measured by the ADCPs (purple arrow) is the sum of the ship-induced flow (green arrow), which is always opposite to the ferry's direction of motion, and the environmental flow (orange arrow) which includes the tides and the wind-induced flow. These two crossings are chosen close to either the maximum flood or ebb when the tidal currents are mostly similar (the magnitude of the orange vector is mostly similar in both crossings).

Hence, the tidal current should have had been underestimated. In contrast, when the ferry sails in the same direction, from Den Helder to Texel (from Texel to Den Helder) but there is an ebb (flood) current, the measured currents should have had a larger magnitude compared to the real currents. When the ferry sails opposite to the tidal current, then the ship-induced backflow strengthens the tidal current. Therefore, the tidal current should have had been overestimated. However, by looking at subplots (c) and (d) in Figure 5.1, we see that this is not the case. During transects 0-8 and 25-31, the magnitudes of the flood tidal currents are overestimated when the ferry sails in the same direction of the current, from Den Helder to Texel (red points). This indicates that the ferry's motion *enhances* the magnitude of the tidal current, in contrast to our expectations. Similar behavior is observed during transects 13-22 when the ebb current dominates.

5.2 Results

Here, we analyze the tidal cycle of the northward velocity in an attempt to investigate whether the strengthening of its magnitude due the ferry's motion is persistent. Subplots (a) and (d) of Figure 5.3 illustrate the northward tidal current measured by the front and rear ADCPs, which is averaged across the inlet (excluding the latitudes near the harbors) and depths as a function of the 32 crossings of the ferry on July 12, 2021. Similar to Figure 5.1, the blue points denote that during those transects, the ferry sails from Texel to Den Helder whereas the orange points denote that the ferry sails from Den Helder to Texel. The black curve corresponds to the fitted curve of the tidal cycle which was found by using harmonic analysis as described in Chapter 2. As we can observe, the blue and the orange points deviate around the black curve, in a systematical manner; the blue points lie below the curve whereas the orange points lie above the curve. This means that this deviation does not depend on the instrument but on the direction the ferry is sailing towards.

In order to compute the deviation/offset of the blue and orange points, we subtract the black curve from those points and the results are shown in Figure 5.3 in subplots (b) and (c) for the front ADCP and subplots (e) and (f) for the rear ADCP. We observe that this deviation slightly oscillates around a mean value. This oscillation may depend on another semi-diurnal tidal component, e.g the solar constituent (S2) that we did not take into account in the harmonic analysis process. The mean value of this difference corresponds to the mean deviation of the measured tidal cycle from the theoretical one. The magnitude of the mean value of the offset is the same for both crossings of the ferry but with opposite signs. This does not have any physical meaning. It is an artifact of our analysis. Also it is worth mentioning that the absolute of the mean deviation of the rear ADCP is larger than the front one. One could expect the opposite result because as the flow approaches the stern, it discharges to the sides of the ferry and as a result the flow along the hull in the direction of motion should reduce (Robijns, 2015). However this is not the case and it remains a difficult to explain observation. Figure 5.4 shows the deviation of the blue and orange points over a month (July 2021). By comparing the two ADCPS, we observe that the rear ADCP has larger deviations compared to the front

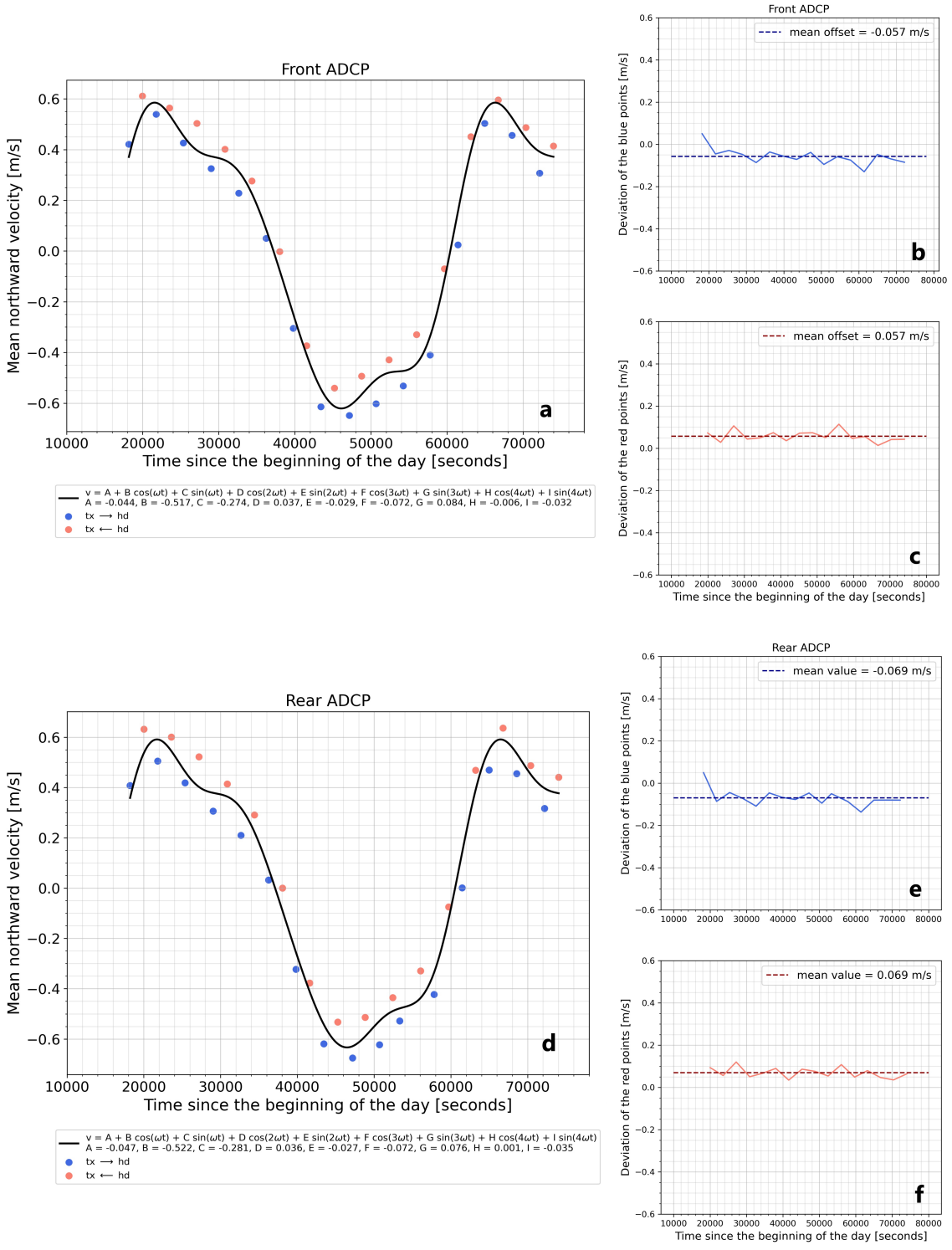

FIGURE 5.3: Subplots (a) and (d) illustrate the northward tidal current measured by the front and rear ADCP, averaged across the inlet (excluding the latitudes near the the harbors) and depths as a function of the 32 crossings of the ferry on July 12, 2021. The blue points indicate that during those transects, the ferry sails from Texel to Den Helder whereas the orange points denote that the ferry sails from Den Helder to Texel. The black curve is the fitted curve of the tidal cycle which was found by using harmonic analysis. Subplots (b) and (c) show the result of the deviation of the blue and the orange points from the fitted line respectively for the front ADCP. Similarly, subplots (e) and (f) show the results for the rear ADCP. The dashed straight lines denote the mean value of the deviations' oscillations.

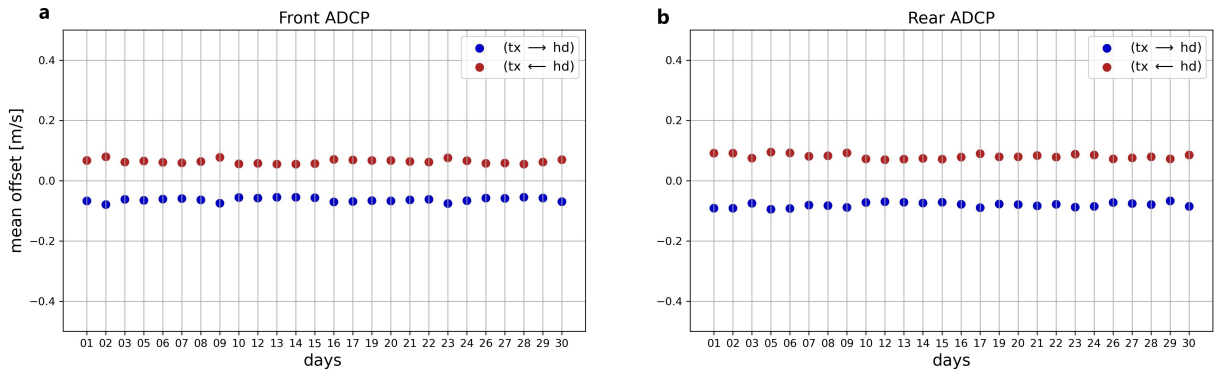

FIGURE 5.4: The mean value of the deviations' oscillations of the blue and orange points over a month (July 2021). The dark blue points denote that during those transects, the ferry sails from Texel to Den Helder whereas the dark red points denote that the ferry sails from Den Helder to Texel.

ADCP. The important thing is that, we see that the deviation of the northward velocity for the two different crossings of the ferry is relatively constant indicating that this phenomenon is persistent over time.

5.3 Discussion

As the observation of a forward flow was not expected, we need to search for its possible origins. We need to understand whether this forward flow comes from an ADCP's error during the measurements, or whether it is an artificial feature due to the ferry's motion or whether it indicates a physical process that we did not consider. In this section we consider three possible origins. Firstly, we investigate whether its origin is an erroneous use of the Doppler-shift formula of the ADCP. This formula is general and it is being used by ADCPs, of all types, but we want to check if it is valid for a moving ADCP as well. However, as we will see that this formula works properly for a moving ADCP, subsequently we refer to other two possible origins of this forward flow: a false measurement of the bottom track velocity or a dragging effect due to ferry's motion.

5.3.1 Investigating the Doppler-shift of a moving ADCP

Generally, all the types of the ADCPs (stanionary or moving) measure the fluid's velocity using the Doppler approach. The transmitted acoustic signal is reflected back by a material which is traveling at the same velocity as the water and through the difference between the transmitted and the reflected acoustic frequency, the water's velocity can be found. According to Mueller et al., 2009, the velocity of the water along the acoustic path for any type of ADCP is computed by the equation:

$$|V| = \frac{C|F_D|}{2F_S} = \frac{C|F_B - F_S|}{2F_S} \tag{5.1}$$

where V is the velocity of the water parallel to the acoustic path, C is the speed of sound in the water, F_S is the frequency of the transmitted acoustic energy, F_B is the frequency of the backscattered acoustic energy and F_D is the Doppler frequency shift. However, for a moving ADCP, we add the correction for its motion by subtracting its velocity from the measurements. One thought is that this formula is not completely correct for a moving ADCP. In the next few paragraphs we analyze the Doppler effects that take place for a moving ADCP in an attempt to check if this equation is valid for a moving ADCP.

In a frame of reference where an observer stands at the harbour, the observer sees that both the ferry/ADCP and the water-flow move. We distinguish the velocity measurements in two phases as illustrated in Figure 5.5. In the first phase, the ADCP sends a sound beam which hits the water particle and in the second phase,

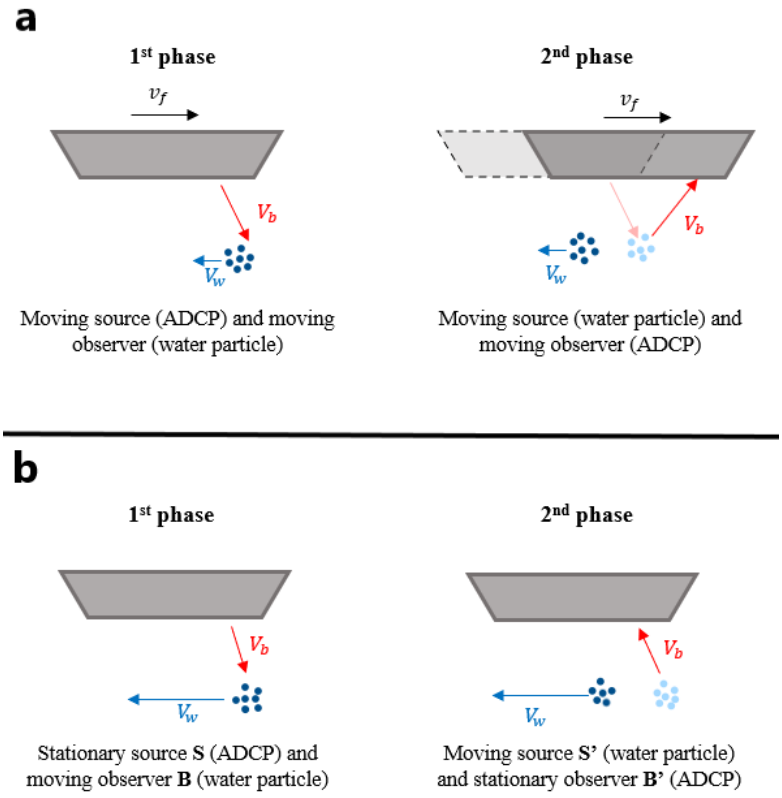

FIGURE 5.5: Illustration of how an ADCP which is located underneath the hull, measures the velocity of water particles according to an observer who stands at the harbour (sketch (a)) and according to the ADCP (sketch (b)). The black vectors (v_f) show the direction of the ferry's motion, the red vectors (V_b) show the direction of the sound beam and the blue vectors (V_w) show the direction of the water particle. The velocity measurements are distinguished in two phases. In the first phase, the ADCP sends a sound beam which hits the water particle and in the second phase, the water particle reflects back to the ADCP the doppler shifted sound beam.

the water particle reflects back to the ADCP the doppler shifted sound beam. In this frame of reference, in both phases we have moving source and moving observer as the sketch (a) in Figure 5.5 shows. Also, as the red arrow notates, the sound beam must change direction to be received by the ADCP. Notice that the beam received by the ADCP is not necessarily the specular[1] reflection of the initial beam because the ADCP is not necessarily moving with the necessary speed to meet the specular reflection. This can be proven by going to the ADCP's frame of reference where the measurements are taken.

In the ADCP's frame of reference, the ADCP sees itself stationary whereas the water particle moves. In the first phase, when the ADCP sends a sound beam, we have a stationary source and a moving observer whereas in the second phase, when the ADCP receives the doppler shifted acoustic beam, we have a moving source and a stationary observer as the sketch (b) in Figure 5.5 shows. In this frame, we can see that for the ship to receive a signal, the reflected signal should travel along the path of the initial beam and thus, it should be a diffuse[2] reflection. Therefore, we don't have an additional doppler effect due to the ship's motion.

[1] Specular reflection occurs when the angle of the reflected signal is the same with the incidence angle.
[2] Diffuse reflection occurs when the incident signal is reflected at many angles rather than at just one angle.

We apply the doppler effect in these two phases to compute the frequency perceived by the observer each time and we obtain eq. (5.2) for the first phase and eq. (5.3) for the second phase.

$$F_B = \frac{C \mp |V|}{C} F_S \tag{5.2}$$

$$F_{B'} = \frac{C}{C \pm |V|} F_{S'} \tag{5.3}$$

The sign above corresponds to the case when the source and the observer move away from each other, whereas the sign below correspond to the case when the source and the observer approach each other. We want to combine these two equations to get an equation for the velocity for the water flow measured by the ADCP in the direction of the acoustic beam. Note that the signal frequency's the moving source sends back to the stationary observer during the second phase is equal to the signal's frequency that the moving observer receives during the first phase: $F'_S = F_B$. Using the argument that the beam path does not change, we obtain:

$$F_{B'} = \frac{C \mp |V|}{C \pm |V|} F_S \tag{5.4}$$

We compute the difference F_D:

$$F_D = F_{B'} - F_S = \frac{C \mp |V|}{C \pm |V|} F_S - F_S = \mp \frac{2F_S|V|}{C \pm |V|} \tag{5.5}$$

We solve for |V| and we obtain:

$$|V| = \frac{\mp F_D C}{F_C + 2F_S} \tag{5.6}$$

This equation differs from the one that the ADCP uses (eq. (5.1))! However, we are going to rewrite eq. (5.6) under the assumption V $\ll$ C. First we solve eq. (5.6) for F_D and we obtain:

$$F_D = \mp \frac{2F_S|V|}{C(1 \pm \frac{|V|}{C})} \tag{5.7}$$

Under the assumption that the water's velocity is much smaller than the sound's velocity, the ratio of the velocities in the denominator can be computed by Taylor approximation, as follows:

$$\frac{1}{1 \pm \frac{|V|}{C}} = \left(1 \pm \frac{|V|}{C}\right)^{-1} \approx 1 \mp \frac{|V|}{C} + O\left(\left(\frac{|V|}{C}\right)^2\right) \tag{5.8}$$

Then we substitute eq. (5.8) into eq. (5.7) by only keeping terms linear in the ratio of the velocities. We then retrieve eq. (5.9).

$$F_D = \mp \frac{2F_S|V|}{C}\left(1 \mp \frac{|V|}{C}\right) \tag{5.9}$$

We solve again for |V| and we obtain:

$$|V| = \frac{C|F_D|}{2F_S} \tag{5.10}$$

Eq. (5.10) is equal to eq. (5.1) and therefore, we agree with the literature's equation only under the assumption that the speed of the flow is much smaller than the speed of sound in the water (V $\ll$ C). It is important to stress that regarding the speed of the sound that the ADCP uses, there is something that it does not consider. The beam of sound is propagating in a non-steady medium, even in the ADCP's frame of reference. Nevertheless, the velocity of the medium has the same order of magnitude as the observer's velocity, and they are much smaller than the order of magnitude of the speed of sound in still water. Therefore this hardly affects our results.

5.3.2 Erroneous determination of the bottom track velocity

Another possible origin for this forward flow in the sailing direction is an erroneous determination of the bottom track velocity. During the time period that the sound beam needs to travel to the seabed and back to the ADCP, the ferry is moving covering a distance. Therefore the angles of the transmitted and the reflected beam differ and as a result this may lead to a misinterpretation of the ADCP about the bottom track velocity. Depending on the beam, this angle of the reflected beam can be larger or smaller than the angle of the transmitted beam. In addition to that, the length of the transmitted and the reflected beam's path differ and consequently the time that the sound needs to travel through these paths vary. Furthermore, we have to keep in mind that the sea-bed along the Marsdiep inlet is not flat but rather it is inclined. This means that the beam's reflection takes place at different depths each time and this affects the path length of the reflected beam. These are the arguments that lead us to conclude that the bottom track velocity could be an origin of error in the velocity measurements. Specifically, as we mentioned in Chapter 2, the bottom track velocity is subtracted from the measured velocities as a correction for the vessel's motion. In this chapter, we found a forward flow instead of a backflow which means that the measured velocities are larger than the real ones, which may indicate that the measured bottom track velocity is smaller than the real one.

5.3.3 Observation of Couette flow

Another possible explanation is that the ferry during its motion displaces a part of the water forward, in the direction of the ferry's motion. According to some engineering studies (Robijns, 2015; Lenselink, 2011; Gourlay, 2006), the flow pattern underneath the hull will resemble Couette flow. Couette flow is the flow between two plates of which one is moving with a constant velocity and the other one is stationary. Therefore, the moving ferry corresponds to the moving plate whereas the bottom bed corresponds to the stationary plate. The Couette flow can be either laminar or turbulent flow, with or without a longitudinal pressure gradient (Schlichting and Kestin, 1961). In the case of the laminar flow where there is no longitudinal pressure gradient present, the velocity decays linearly. When the flow becomes turbulent or the longitudinal pressure gradient is present, the velocity profile behaves differently. In the case of the moving ferry over the bed, the flow is turbulent and it is influenced by a longitudinal pressure gradient. At the bow of the ferry, the pressure is high while, at the stern, there is an area of low pressure in front of the propeller. Therefore a pressure distribution is generated beneath the hull resulting in a positive pressure gradient. This positive pressure gradient influences the motion of the flow and it also drives a part of the flow beneath the hull. Figure 5.6 shows the effect of dragging action of the moving plate exerted on the fluid particles for a positive pressure gradient. Near the moving plate (moving ferry), the fluid follows the motion of the plate. For small positive pressure gradients (subfigure (a) in Figure 5.6), this forward motion of the fluid weakens as the depth increases whereas for large positive pressure gradients (subfigure (b) in Figure 5.6), a backflow may

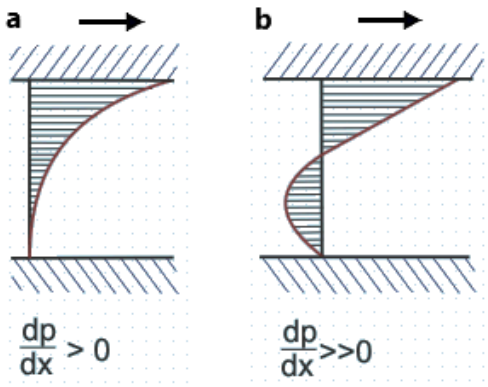

FIGURE 5.6: Velocity profile for the Couette flow for turbulent flow with positive pressure gradient. The figure was retrieved by Mathur, Jajal, and Singh, 2017.

occur near the stationary plate (seabed) which is at rest. This might explain the net depth-averaged forward motion of the current, in the direction of the ferry's motion. We would expect that the magnitude of the forward velocity of the currents would have had the same order of magnitude as the ferry's speed (4-5 m/s), as this is what happens in the Couette flow model (Robijns, 2015) i.e the velocity at the top is exactly equal to the plate's velocity (we of course relax this demand by only expecting the magnitudes to be equal, not the values themselves). However Figure 5.4 indicates that the magnitude of the net depth- and cross-section averaged forward velocity of the currents is around 0.06 m/s. There are two possible explanations; either the magnitude of the backflow is of the same order of magnitude as the environmental flow's speed or the ferry drags along each water particle, accelerating them towards the sailing direction, but since the ship will not keep its contact with the same water particles for long, they are being accelerated for a very small amount of time thus, the water particles do not reach velocity values of magnitudes comparable to that of the ferry.

Chapter 6

Conclusions and Outlook

This research project focused on the analysis of the temporal and spatial variability of the velocity field of the flow along the Marsdiep inlet. This was achieved by using two hull-mounted ADCPs; one of the two ADCPs was mounted at the front and the other one at the rear of the TESO ferry. In the first part of this study, our goal was to familiarize ourselves with the data and to extract information about the tidal currents and their features, and about the variations of the tidal profiles. By investigating the tidal cycle across the inlet, we managed to identify the tidal asymmetry which is observed in other studies (Sassi et al., 2016; de Vries, 2015; Buijsman, 2007) with a small floodward residual current along the Den Helder coastline and a large ebbward residual current along the Texel coastline. Also we extracted the phase difference between the water elevation and the tidal current. The phase lag between the two curves was found to be 60-70° indicating that the semi-diurnal tidal waves in the Marsdiep channel are both partially progressive and standing as we expected from the literature (Groeskamp, 2008).

Furthermore, we exploited the fact that two ADCPs are mounted on the ferry to search for evidence of turbulence. The features of tidally induced turbulence were identified from the noise of the measurements of the horizontal velocities measured by the two ADCPs. We infer that the instrumental noise level might approximately be 0.2 ± 0.01 m/s and that tidally induced turbulence further raises the value of the noise above 0.2 m/s by a maximum of 0.1 m/s. The instrumental noise level is fairly high and although we achieved to extract information about the physical noise (turbulence), it should reduce to get better results and this is what Soons, 2022 achieved to do in his recent study by applying mass constraints. Furthermore, we managed to relate turbulence with the strength and the phase of the tide and to construct the structure of turbulence over the depth. We found that the flood current carries larger turbulence than the ebb current due to the former being stronger than the latter. Moreover, the fact that the tidally induced turbulence reaches larger values during the decelerating phase of the tide is possibly caused by a time delay for the turbulence to express itself along the water column. It starts being generated near the seabed during the early stage of the accelerating phase of the tide. As the tidal current becomes stronger, turbulence increases and it is transferred in the whole water column. The decelerating part of the cycle carries some turbulence which starts dissipating. In addition, we found that the tidally induced turbulent features increase with increasing depth with a sharp reduction near the seabed as we expected due to the dominance of the shear stress there. The friction effects set the current velocity to zero near the bottom preventing the generation of turbulence which finally manages to become manifest a little higher, at the edge of the boundary layer. Finally we have to keep in mind that the turbulent features that we observed are limited below the ferry and in the space between the two ADCPs, and that we do not have a complete view of the turbulence along the inlet. Also, it is important to stress that for this analysis, we compared the horizontal velocities at each measured latitudinal location with an average time difference between the measurements of the two ADCPs of 30s. Another suggested approach for further study on turbulence would be to compare the horizontal velocities that are measured simultaneously by the two ADCPs with roughly 100m distance between them.

During the second part of this study, our goal was to search for the influence of the ship's motion on the vertical and the along-ship horizontal velocity measurements. Regarding the measured vertical velocity, we identified its linear decay over depth and we managed to relate it to the ferry's speed. Although its linear dependence with depth was expected due to the shallow-water theory, subplots (a) and (b) in Figure 4.10 which illustrate the averaged vertical velocity along the inlet as a function of depth, show that the maximum

of the vertical velocity lies at a depth of 7-8m instead of at the surface as the shallow water theory predicts. Therefore the function which corrects the vertical velocity for the ferry's speed (eq. (4.3)) is not entirely correct because it does not work properly for all depths but in this study we restrained ourselves to the assumption of the linear dependency.

Subsequently we worked with three candidate correction schemes on the vertical velocity, based on these findings. The first correction (C1) was based on the elimination of the net vertical transport of the water, by setting the mean value of the vertical velocity to zero. In the second correction (C2), we corrected the vertical velocity profile for the ferry's velocity by using the ferry's velocity function of eq. (4.3). The third correction (C3) is a combination of schemes C1 and C2; by applying the function of the ferry's velocity to the corrected vertical current velocities from the C1 scheme, we end up with the C3 corrected data. After applying these corrections, we concluded that C3 was the best correction scheme. Also, by comparing the corrected velocities of the front and the rear ADCP we found that the result for the front ADCP looks more reliable than the rear's one. Through the corrected velocity of the front ADCP we found realistic vertical velocities induced by the horizontal flow over a sloping bottom and we were able to give a physical interpretation of the vertical velocity by identifying physical features such as "boils" and fronts. This correction seems to be working well enough locally in the presence of local phenomena, e.g "boils", but fails in the presence of large scale phenomena like estuarine circulations. Nevertheless, the correction procedure as developed in the present study could be considered as a good start for further research on the correction of the vertical velocity of the flow. One suggestion for future research would be to compare the present data with in situ (mooring) data. The in situ measurements for the vertical velocity could be used as a reference for specific locations along the transect. These locations must be chosen such that there is a high probability that the ferry will pass directly over them. Then by comparing this reference data with the data extracted by the hull-mounted ADCPs, the influence of the ferry's motion in the vertical velocity could possibly be identified and eliminated from the contaminated data.

Lastly, regarding the along-ship horizontal velocity, we could not manage to identify a ferry-induced backflow as we expected due to the motion of the water which must flow in the opposite direction of the sailing direction to fill the empty space the ship leaves in its passing. In contrast, we observed a forward flow in the direction of the ferry's motion. We discussed a number of potential causes (e.g erroneous determination of the bottom track velocity, presence of couette flow), but none of them could explain this observation in its entirety. Therefore, further research is needed in order to understand the influence of the ferry's motion on the velocity components in the sailing direction. A way to check if there is an erroneous determination of the bottom track velocity is to correct the flow profiles for vessel motion by using the global positioning system (GPS) and gyrocompass (although the gps-derived velocities contain a substantial level of noise). In addition, laboratory experiments could be carried out to investigate the velocity field of the flow affected by the motion of a ship in calm water.

Bibliography

Aardoom, J. H. and Mol, J. (2006). "Quantification of sediment concentrations and fluxes from ADCP measurements". In: *Evolutions in hydrography, 6th-9th November*, pp. 166–171.

Buijsman, M. C. and Ridderinkhof, H. (2008). "Long-term evolution of sand waves in the Marsdiep inlet. II: Relation to hydrodynamics". In: *Continental Shelf Research* 28.9, pp. 1202–1215.

Buijsman, M. C. (2007). "Ferry-observed variability of currents and bedforms in the Marsdiep inlet". PhD thesis. Utrecht University.

Buijsman, M. C. and Ridderinkhof, H. (2007). "Long-term ferry-ADCP observations of tidal currents in the Marsdiep inlet". In: *Journal of Sea Research* 57.4, pp. 237–256.

Cengel, Y. and Cimbala, J. (2013). *EBOOK: Fluid Mechanics Fundamentals and Applications (SI units)*. McGraw Hill.

Cushman-Roisin, B. and Beckers, J.-M. (2011). *Introduction to geophysical fluid dynamics: physical and numerical aspects*. Academic press.

Deines, K. L. (1999). "Backscatter estimation using broadband acoustic Doppler current profilers". In: *Proceedings of the IEEE Sixth Working Conference on Current Measurement (Cat. No. 99CH36331)*. IEEE, pp. 249–253.

de Vries, J. (2015). "On the local dynamics of currents in the estuarine Marsdiep basin". PhD thesis. Utrecht University.

Doonan, I. J., Coombs, R. F., and McClatchie, S. (2003). "The absorption of sound in seawater in relation to the estimation of deep-water fish biomass". In: *ICES Journal of Marine Science* 60.5, pp. 1047–1055.

Elias, E., Pearson, S., and van der Spek, A. (2020). "Understanding the Morphological Processes at Ameland Inlet–Kustgenese 2.0 Synthesis of the Tidal Inlet Research". In: *Deltare s Rapport*, pp. 1220339–008.

Elias, E. P. and van der Spek, A. J. (2017). "Dynamic preservation of Texel Inlet, the Netherlands: understanding the interaction of an ebb-tidal delta with its adjacent coast". In: *Netherlands Journal of Geosciences* 96.4, pp. 293–317.

Elias, E. P., van der Spek, A. J., Wang, Z. B., and De Ronde, J. (2012). "Morphodynamic development and sediment budget of the Dutch Wadden Sea over the last century". In: *Netherlands Journal of Geosciences* 91.3, pp. 293–310.

Ghaffari, P., Azizpour, J., Noranian, M., Chegini, V., Tavakoli, V., and Shah-Hosseini, M. (2011). "Estimating suspended sediment concentrations using a broadband ADCP in Mahshahr tidal channel". In: *Ocean Science Discussions* 8.4, pp. 1601–1630.

Gilcoto, M., Jones, E., and Fariña-Busto, L. (2009). "Robust estimations of current velocities with four-beam broadband ADCPs". In: *Journal of Atmospheric and Oceanic Technology* 26.12, pp. 2642–2654.

Gourlay, T. (2006). "Flow beneath a ship at small underkeel clearance". In: *Journal of ship research* 50.03, pp. 250–258.

Groeskamp, S. (2008). "Solitary Internal Waves in Marsdiep Tidal Channel". MA thesis. Utrecht University.

Guo, L., Wang, Z. B., Townend, I., and He, Q. (2019). "Quantification of tidal asymmetry and its nonstationary variations". In: *Journal of Geophysical Research: Oceans* 124.1, pp. 773–787.

Haught, D., Venditti, J. G., and Wright, S. A. (2017). "Calculation of in situ acoustic sediment attenuation using off-the-shelf horizontal A DCPs in low concentration settings". In: *Water Resources Research* 53.6, pp. 5017–5037.

Khojasteh, D., Hottinger, S., Felder, S., De Cesare, G., Heimhuber, V., Hanslow, D. J., and Glamore, W. (2020). "Estuarine tidal response to sea level rise: The significance of entrance restriction". In: *Estuarine, Coastal and Shelf Science* 244, p. 106941.

Kostaschuk, R., Best, J., Villard, P., Peakall, J., and Franklin, M. (2005). "Measuring flow velocity and sediment transport with an acoustic Doppler current profiler". In: *Geomorphology* 68.1-2, pp. 25–37.

Lenselink, R. (2011). "Interaction between loaded barges and bed material". MA thesis. Delft University of Technology.

Lerczak, J. A. and Geyer, W. R. (2004). "Modeling the lateral circulation in straight, stratified estuaries". In: *Journal of Physical Oceanography* 34.6, pp. 1410–1428.

Maas, L. R. M. (2019). *Lecture notes for course Wave attractors at Utrecht University*.

Maas, L. and van Haren, J. (1987). "Observations on the vertical structure of tidal and inertial currents in the central North Sea". In: *Journal of Marine Research* 45.2, pp. 293–318.

Mathur, M., Jajal, N. A., and Singh, R. K. (2017). "Finite difference solver for couette flow with applied pressure gradients". In: *International Journal of Advance Research and Innovation* 5.2, pp. 247–250.

Medwin, H. and Clay, C. S. (1998). *Fundamentals of acoustical oceanography*. Elsevier.

Meteorological Service of Canada, (2004). *Procedures for the Review and Approval of ADCP Discharge Measurements: Water Survey of Canada*. URL: https://library.wmo.int/doc_num.php?explnum_id=4769.

Mueller, D. S., Wagner, C. R., Rehmel, M. S., Oberg, K. A., and Rainville, F. (2009). *Measuring discharge with acoustic Doppler current profilers from a moving boat*. US Department of the Interior, US Geological Survey Reston, Virginia (EUA).

Nauw, J., Merckelbach, L., Ridderinkhof, H, and van Aken, H. (2014). "Long-term ferry-based observations of the suspended sediment fluxes through the Marsdiep inlet using acoustic Doppler current profilers". In: *Journal of Sea Research* 87, pp. 17–29.

Neill, S. P. and Hashemi, M. R. (2018). "Chapter 7 - In Situ and Remote Methods for Resource Characterization". In: *Fundamentals of Ocean Renewable Energy*. Ed. by S. P. Neill and M. R. Hashemi. E-Business Solutions. Academic Press, pp. 157–191. ISBN: 978-0-12-810448-4. DOI: https://doi.org/10.1016/B978-0-12-810448-4.00007-0. URL: https://www.sciencedirect.com/science/article/pii/B9780128104484000070.

Ponsoni, L., Nichols, C., Buatois, A., Kenkhuis, J., Schmidt, C., de Haas, P., Ober, S., Smit, M., and Nauw, J. J. (2019). "Deployment of a floating tidal energy plant in the Marsdiep inlet: resource assessment,

environmental characterization and power output". In: *Journal of Marine Science and Technology* 24.3, pp. 830–845.

Ralston, D. K. and Stacey, M. T. (2005). "Longitudinal dispersion and lateral circulation in the intertidal zone". In: *Journal of Geophysical Research: Oceans* 110.C7.

Robijns, T. (2015). "Flow beneath inland navigation vessels". MA thesis. Delft University of Technology.

Sassi, M. G., Gerkema, T., Duran-Matute, M., and Nauw, J. J. (2016). "Residual water transport in the Marsdiep tidal inlet inferred from observations and a numerical model". In: *Journal of Marine Research* 74.1, pp. 21–42.

Schlichting, H. and Kestin, J. (1961). *Boundary layer theory*. Vol. 121. Springer.

Soons, J. (2022). "Applying Mass Conservation to ADCP-data". MA thesis. Utrecht University.

Stacey, M. T., Monismith, S. G., and Burau, J. R. (1999). "Measurements of Reynolds stress profiles in unstratified tidal flow". In: *Journal of Geophysical Research: Oceans* 104.C5, pp. 10933–10949.

Teledyne RD Instruments, (2011). *Acoustic Doppler Current Profiler: Principles of operation.* URL: `https://www.comm-tec.com/Docs/Manuali/RDI/BBPRIME.pdf`.

Thorpe, S., Green, J., Simpson, J., Osborn, T., and Smith, W. N. (2008). "Boils and turbulence in a weakly stratified shallow tidal sea". In: *Journal of physical oceanography* 38.8, pp. 1711–1730.

Trauthwein, G. (October 2019). "C-Job CEO Cofounder, Basjan Faber, Born to Design". In: *Maritime Reporter and Enginnering News* 81.10, pp. 34–39.

van Haren, H., Oakey, N., and Garrett, C. (1994). "Measurements of internal wave band eddy fluxes above a sloping bottom". In: *Journal of Marine Research* 52.5, pp. 909–946.

Wang, Z. (2018). *Long term morphological development of the tidal inlet systems in the Dutch Wadden Sea*. URL: `https://www.helpdeskwater.nl/@205195/long-term/`.

Wang, Z., Hoekstra, P, Burchard, H, Ridderinkhof, H, Swart, H. de, and Stive, M. (2012). "Morphodynamics of the Wadden Sea and its barrier island system". In: *Ocean & coastal management* 68, pp. 39–57.

Ward, S. L., Robins, P. E., Lewis, M. J., Iglesias, G., Hashemi, M. R., and Neill, S. P. (2018). "Tidal stream resource characterisation in progressive versus standing wave systems". In: *Applied energy* 220, pp. 274–285.